

The effects of electroadhesive clutch design parameters on performance characteristics

Stuart B Diller¹ , Steven H Collins^{1,2,3} and Carmel Majidi^{1,3}

Abstract

Actuators that employ clutches can exhibit mechanical impedance tuning and improved energy efficiency. However, these integrated designs have been difficult to achieve in practice because traditional clutches are typically heavy and consume substantial power. In this article, we describe a lightweight and low-power clutch that operates with electrostatic adhesion and achieves order-of-magnitude improvements in performance compared to traditional clutches. In order to inform appropriate design in a variety of applications, we experimentally determine the effect of clutch length, width, dielectric thickness, voltage, and electrode stiffness on the holding force, engage and release times, and power consumption. The highest performance clutch held 190 N, weighed 15 g, and consumed 3.2 mW of power. The best samples released and engaged within 20 ms, as fast as conventional clutches. We also conducted a fatigue test that showed reliable performance for over 3 million cycles. We expect electroadhesive clutches like these will enable actuator designs that achieve dexterous, dynamic movement of lightweight robotic systems.

Keywords

Electroadhesive clutch, electroadhesion, clutch, transmission, actuator

Introduction

Roboticians use clutches to reduce the energetic cost of actuation and achieve more versatile behavior by controlling how force and mechanical energy are transmitted in a system (Plooij, 2015). Many actuator designs improve energy efficiency by selectively engaging springs that use passive mechanics to exert force (Figure 1(a)) (Collins et al., 2005, 2015; Elliott et al., 2013; Rouse et al., 2014; Wu and Lin, 2017). Clutches also enable hybrid actuation schemes that can operate in multiple torque and speed regimes, for example, by employing motors with dramatically different gearing ratios (Figure 1(b)) (Girard and Asada, 2016; Mathijssen et al., 2016). Alternatively, they allow for a single actuator to actuate many degrees of freedom with a one-to-many architecture (Figure 1(c)) (Hawkes et al., 2016; Hunt et al., 2013). Discrete stiffness tuning has been demonstrated with clutches to control mechanical interaction with humans in haptics applications (Figure 1(d)) (Awad et al., 2016; Rossa et al., 2014; Sakaguchi et al., 2001). However, designers are challenged by the relatively high mass and power consumption of traditional active clutches that rely on solenoids, such as electromagnetic or magnetorheological clutches (Rouse et al., 2014; Shafer and Kermani,

2011). Electrorheological clutches activate with directly applied voltage instead of a solenoid, but require thousands of volts and struggle to achieve high forces (Boku and Nakamura, 2010; Furusho et al., 2002; Sakaguchi et al., 2001). Passively locking devices eliminate the need for power input, but come with kinematic and control limitations and typically need to be customized for each application (Collins et al., 2015; Hawkes et al., 2016). Hydraulic layer-jamming devices achieve high forces with low weight and low theoretical power consumption, but take seconds to change states and require an accompanying compressor (Choi et al., 2018). Fluidic matrix composites can quickly change stiffness, but require valves to operate and have relatively high off-state stiffness (Shan et al., 2009). While the potential benefits of actuators that employ clutches

¹Department of Mechanical Engineering, Carnegie Mellon University, Pittsburgh, PA, USA

²Department of Mechanical Engineering, Stanford University, Stanford, CA, USA

³The Robotics Institute, Carnegie Mellon University, Pittsburgh, PA, USA

Corresponding author:

Stuart B Diller, Department of Mechanical Engineering, Carnegie Mellon University, 5000 Forbes Avenue, Pittsburgh, PA 15213, USA.
Email: sdiller@andrew.cmu.edu

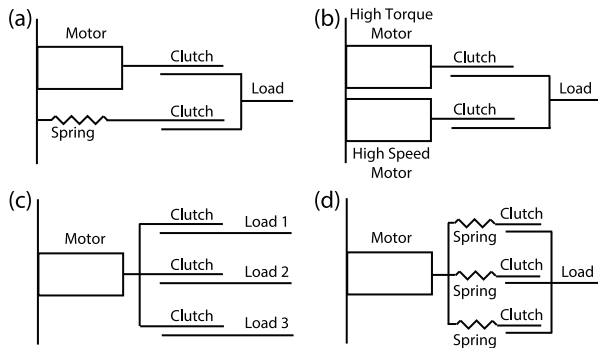


Figure 1. Alternative actuator configurations using: (a) clutchable motor and spring in parallel; (b) transmission with selectable motor; (c) one-to-many transmission; (d) transmission with variable series elasticity.

are appealing, implementation with available clutches remains challenging.

Controllable electrostatic adhesives display promising characteristics for translation into a clutching device. Compared to other clutching materials, electroadhesive films can be very lightweight and require very little power in order to form strong bonds with other surfaces (Guo et al., 2017; Prahlad et al., 2008). Holding forces over 100 kPa have been reported (Chen and Bergbreiter, 2017), and reliable adhesion to various substrates has been demonstrated (Guo et al., 2018; Kakinuma et al., 2010; Ruffatto et al., 2014). However, these devices are designed to adhere to substrates, as in applications such as robotic wall-climbing, and additional mechanisms and hardware must be incorporated to achieve a self-contained clutch. Previous attempts to create clutches that employ electroadhesion had only limited success because of slow response times and significant force hysteresis (Aukes et al., 2014; Karagozler et al., 2007), which are due mainly to materials selection and mechanical design. We previously improved on this work by designing and demonstrating an electroadhesive clutch that produced high forces with much lower mass and power consumption than conventional clutches while achieving comparable response times and controllability (Figure 2) (Diller et al., 2016). However, this study lacked a systematic investigation of the relationship between clutch design and performance. For instance, knowing the effect of increasing clutch area or applied voltage on force and clutch responsiveness would enable us to make informed design decisions for an application requiring 10 times higher force than what we have previously demonstrated. Without a broad knowledge of the effects of design choices, generalization of electroadhesive clutches to many usage cases would be slow and difficult.

In this article, we perform a systematic experimental investigation of electroadhesive clutch design in order

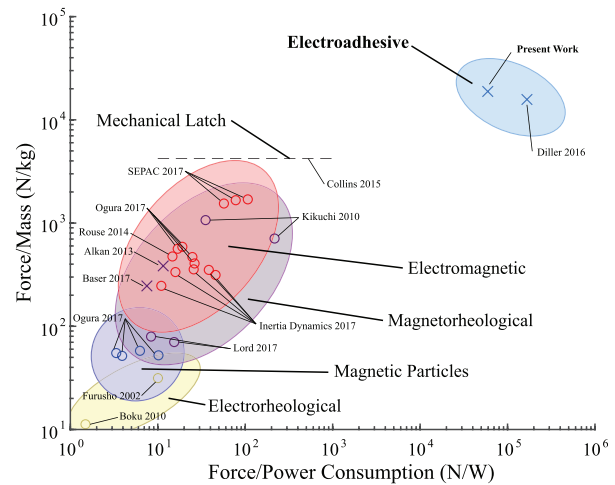


Figure 2. Comparison of mass and power consumption based on clutch mechanism. An “x” indicates a linear clutch, and an “o” indicates a rotary clutch. The torque of rotary clutches was converted to force by dividing by the radius of the clutch plate. Active clutches were only included if the force (or torque), mass, and power could be calculated or estimated from empirical data. The mechanical latch is shown as a dashed line because it consumes no power, but is not electrically controllable. The electroadhesive clutch achieves order-of-magnitude improvements in performance compared to traditional clutches. Source: Alkan et al., 2013; Baser et al., 2017; Inertia-Dynamics, 2017; Kikuchi et al., 2010; Lord, 2017; Ogura-Industrial-Corp, 2017a; Ogura-Industrial-Corp, 2017b.

to better inform implementation in future applications. Our goal is to establish a comprehensive set of design principles that can be used to employ electroadhesive clutches in a broad range of applications, as well as to direct further improvement of clutch performance.

Design overview

Working principle

The electroadhesive clutch is composed of two separate clutch plates (Figure 3(a) to (c)). Each plate is an aluminum-sputtered polymer electrode coated with a high-dielectric insulator (Luxprint, Dupont). The plates are flexible, so the necessary structure and load distribution are achieved by attaching them to stiff carbon fiber bars with thin double-sided acrylic tape. The two clutch plates are oriented such that their dielectric layers are in contact, and small rubber bands serve as tensioners to maintain the correct configuration in any orientation. Applying a voltage across the electrodes causes opposite electric charges to accumulate on the electrode surfaces. As the charge increases, an electrostatic attraction develops at the interface and the plates adhere to one another. When the carbon fiber attachments of each clutch plate are pulled away from one another, the adhesion and friction at the interface of the clutch plates cause a shear force that resists relative motion.

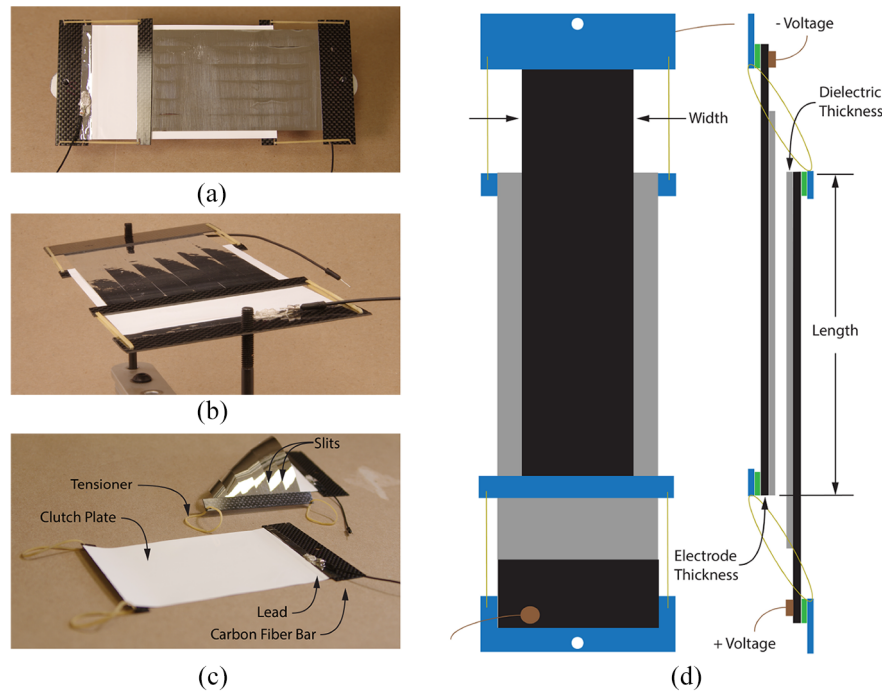


Figure 3. Electroadhesive clutch. (a, b) The clutch in its operating configuration and (c) clutch components. The clutch is composed of two clutch plates attached to carbon fiber bars and held in place by small tensioners. (d) Diagram of clutch parameters. In this study, the width, length, electrode thickness, dielectric thickness, and voltage are systematically varied.

Discharging the electrodes eliminates the electrostatic attraction at the interface of the clutch plates, allowing them to release and slide freely. The operation of the clutch is illustrated in the “Electroadhesive Clutch Demonstration” video (Supplemental Material).

Fabrication

The clutch plates were created by coating layers of an insulating ceramic-polymer composite (Luxprint; Dupont Microcircuit Materials, Research Triangle Park, NC) onto aluminum-sputtered BOPET (bi-axially oriented polyethylene terephthalate) film, which served as the electrode. The 25- and 100- μm -thick films were sourced from Nielsen Enterprises (Kent, WA), and the 50- and 125- μm -thick films were sourced from McMaster-Carr (Aurora, OH). The McMaster-Carr films were of generally higher quality, but were only available in 50 and 125 μm thicknesses. The aluminum coating of the BOPET served as the conducting surface for the electrode, while the polymer portion of the BOPET served as a backing to the aluminum and transmitted force from the interface of the two clutch plates to the carbon fiber bars. Changing the thickness of the BOPET was accomplished by changing the polymer backing thickness and had no effect on the ability of the aluminum layer to provide an electrically conductive electrode surface. Instead, the thicker electrodes provided a stiffer connection between the clutch interface

and the carbon fiber and made the overall clutch plate thicker and stiffer. While only the surface aluminum layer conducts electricity, we refer to the entire aluminumized BOPET film as the electrode in this article. To coat the uncured Luxprint onto the conductive aluminum BOPET surface, we first taped one edge of a 15" square BOPET film onto an 18" square first surface flatness mirror (First Surface Mirror LLC, Toledo, OH), such that the entire BOPET film rested on the mirror. Uncured Luxprint was deposited along a line near the taped edge, and a 13-, 20-, or 27- μm profile rod (Zehntner GmbH Testing Instruments, Sissach, Switzerland), depending on the desired coating thickness, was pulled across the surface away from the taped edge. The coated film was immediately baked in a 1.9 cubic foot ventilated oven (Across International, Livingston, NJ) at 130°C under vacuum for 2 h. The film was then removed and cooled at room temperature. After waiting at least 5 h, the film was put back into the oven to bake for two more hours under the same conditions. The resulting thickness of the dielectric layer was approximately 10, 18, or 25 μm , depending on the profile rod used and the speed and pressure applied during spreading of the uncured Luxprint. To create dielectric layers thicker than 25 μm , the coating process was repeated on top of the previously baked dielectric layers, until the desired thickness was achieved.

The coated electrodes were cut to size using a rotary cutter (Fiskars, Helsinki, Finland). If the sample did

not have any uncoated surface of the BOPET for electrical contact, acetone was used to remove Luxprint from a small area. The electrodes were then attached to carbon fiber shims using a polyacrylate adhesive (VHB, 3M, Maplewood, MN). Silver particle-based conductive epoxy (MG Chemicals, Burlington, Canada) was used to make electrical contact between ring terminals and the conductive BOPET surface. The epoxy was cured by placing the entire clutch in the oven at 65°C for 1 h under atmospheric pressure. Tensioning rubber bands (Pale Crepe Gold; Alliance, Hot Springs, Arkansas) were fitted into slots cut in the carbon fiber and glued in place on the electrode side using cyanoacrylate glue. For every clutch, both BOPET electrodes were coated with Luxprint so that the total dielectric thickness was the sum of the thicknesses of the coatings on each electrode. The alignment springs were attached via slots to the other clutch plate, such that the dielectric coatings contacted one another. One coated electrode was cut to be 1 cm wider than the other, to prevent shorting between the edges of the electrodes. An overview of the fabrication process can be viewed in the “Electroadhesive Clutch Fabrication” video (Supplemental Material).

Experimental design

The aim of this study is to gain answers and insights into the following design questions:

- Can clutch area be effectively scaled up or down for various applications, and what are the effects of changing its size?
- How much dielectric and electrode material are needed, and will less material necessarily achieve better holding force to weight ratios?
- How does operating voltage affect the holding force and power consumption?
- What factors contribute to reliable and fast release and engage?
- How long can electroadhesive clutches last under constant operation?

To answer these questions, we conducted an extensive characterization of clutch performance as a function of the design parameters. Using these results, we endeavor to provide practical guidelines and confidence to designers considering using electroadhesive clutches in their actuation schemes. Each experimental results section will lead the reader through the definition of a performance outcome, interpretation of the data, and how the results inform future designs. Next, we present an empirical model of clutch holding force derived from our experimental data and compare it to predictions from theory. Finally, we provide a design example and discuss the suitability of electroadhesive clutches for applications in robotics and beyond.

The design parameters varied in this study are illustrated in Figure 3(d). Clutches have various widths, with one clutch plate slightly wider in order to prevent shorts across the edges of the electrodes. “Clutch length” refers to the overlapping length between the two clutch plates and is adjustable by changing the distance between the bolt attachment points before activation. The dielectric thickness and electrode thickness are varied independently, in order to separately investigate the effect of the separation distance between electrodes and the overall thickness and stiffness of the clutch plates. Finally, we vary the magnitude of the voltage applied across the electrodes of the two clutch plates.

A common theoretical model for predicting the maximum shear force in electroadhesive devices is given by the equation

$$F_x = \frac{\mu \cdot \epsilon \cdot \epsilon_0 \cdot A \cdot V^2}{2 \cdot d^2} \quad (1)$$

where μ is the coefficient of friction, ϵ is the relative permittivity of the dielectric, ϵ_0 is the electric constant, A is the interface area, V is the voltage, and d is the thickness of the dielectric (Chen and Bergbreiter, 2017). We chose our design parameters to encompass most of the variables in this equation in order to facilitate a meaningful evaluation of the applicability of this theory to the performance of our device.

In the following section, we report measurements of the maximum holding force, release time, engage time, and power consumption of electroadhesive clutches as a function of clutch length, width, dielectric thickness, electrode thickness, and applied voltage. The maximum holding force is determined in a materials testing machine by increasing tension in the clutch until slipping occurs. We measure release and engage time by observing the changes in force and stiffness as the clutch is activated and deactivated under load. We determine the power consumption by measuring the capacitance and leakage current of the clutches at high voltage. Finally, we show the results of a fatigue life test conducted by repeatedly activating and loading the clutches.

Experimental characterization

Holding force

Holding force methods. The maximum clutch force before slip as a function of clutch width, length, dielectric thickness, electrode thickness, and voltage was determined using a materials testing machine (Instron 5969; Instron, Norwood MA). For each test, the clutch was loaded into the testing machine and voltage was applied using a high-voltage power supply (Model PS375; Stanford Research Systems, Sunnyvale, CA) to initiate adhesion. After waiting for 1 s to ensure full

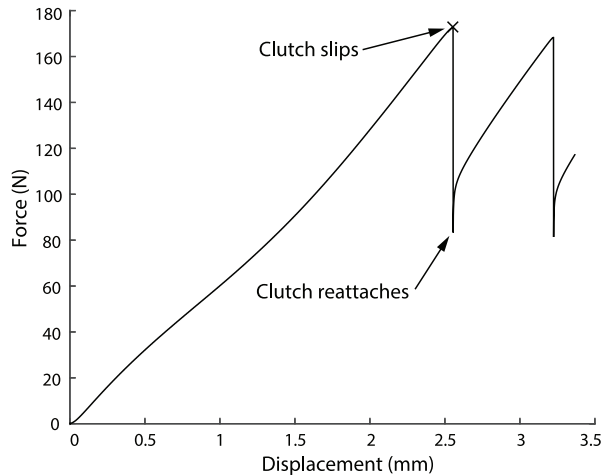


Figure 4. A representative maximum holding force test. After slipping, the clutch immediately reattaches at a lower force because the voltage is still being applied. The slipping force slowly decreases as more slips occur, because the clutch overlap length decreases by a small amount after each slip.

engagement, the testing machine strained the clutch at 10 mm/min until at least two slips occurred (Figure 4). The highest force value observed was recorded as the maximum holding force. In the vast majority of cases, the maximum holding force was observed just before the first slip. In the remaining cases, the first slip occurred at a lower force because of a short through the dielectric layer. Pilot testing showed that the maximum holding force reached a steady-state value after about three consecutive tests. Based on this result, we conducted six consecutive tests on each clutch at each condition, with about 10 s between tests. The maximum holding forces from only the last three tests were included in the dataset. With the exception of the multi-parameter dielectric thickness and voltage sweep, three separate clutches were tested at each condition. Because the final dielectric thickness was difficult to precisely control during fabrication, we decided to test many clutches with many distinct dielectric thicknesses for the two-dimensional (2D) dielectric thickness and voltage sweep, as opposed to making three identical clutches at each of a few dielectric thicknesses. The thickness of the dielectric coating of each clutch plate was measured four times at each corner using a micrometer (Mitutoyo IP65; Mitutoyo, Kawasaki, Japan) that has a resolution of 1 μm . The reported dielectric thickness of each clutch was calculated by adding the thicknesses of the dielectric coatings on the two electrodes to find the total thickness of dielectric material separating the electrode surfaces. The clutches tested in the sweep of area had 50- μm -thick electrodes, dielectric thickness of $36 \pm 2.9 \mu\text{m}$, and were activated with 250 V. The clutches tested in the sweep of dielectric thickness and voltage had 50- μm -thick electrodes, 10 cm overlap length, and 8 cm width. The clutches

tested in the sweep of electrode thickness and length had dielectric thickness of $36.6 \pm 3.9 \mu\text{m}$, 8 cm width, and were activated with 250 V. Test order for all conditions on each clutch was randomized. Clutches were rested for at least 3 h between measurements.

The maximum holding force was also tested as a function of time. For each test, the clutch was loaded into a materials testing machine (Instron 4469; Instron, Norwood MA; MTS ReNew Upgrade, MTS, Eden Prairie, MN), and a voltage of 250 V was applied with the high voltage power supply. The clutch was left activated for a predetermined amount of time that was varied between tests. Then the clutch was displaced at 240 mm/min, causing the clutch to slip within 200 ms. The highest force value observed was recorded as the maximum holding force for that amount of activated time. We tested six clutches at 1, 3, 10, and 30 s activated time conditions. Each clutch was tested six times at each condition, and the last three tests were included in the dataset. The order of activation time conditions was randomized for each clutch. The clutches tested encompassed a range of clutch parameter values, including 25 and 50 μm electrodes, dielectric thicknesses between 22 and 92 μm , and overlap lengths of 8 and 14 cm. The maximum holding forces from all tests of each clutch were divided by the average maximum holding force of the 30-s activated time condition for that clutch. These normalized values were averaged, and the error bars indicate the standard deviation of the combined set of normalized values from all six clutches.

Holding force results. Maximum clutch holding force increases approximately linearly with area for a large range of areas and aspect ratios (Figure 5(a)). Dielectric thickness has a non-monotonic influence on maximum holding force (Figure 5(b)). Holding force peaks in the 50–80 μm region, with large drop-offs as the thickness becomes larger or smaller. Across all dielectric thicknesses, holding force rises dramatically as applied voltage is increased. The maximum holding force rises moderately as electrode thickness decreases (Figure 5(c)). Increasing length causes a linear increase in force independent of electrode thickness. The maximum clutch holding force increases as the amount of time the clutch is activated increases (Figure 6).

Holding force design insights. These results indicate that clutch force is maximized by clutch plates with 25- μm -thick electrodes and dielectric thicknesses in the 50- to 80- μm range. Further decreasing the electrode stiffness could increase maximum holding force. However, the yield strength of the BOPET material may begin to restrict the operating force of the clutch. For example, an 8-cm-wide clutch with 25 μm electrodes is expected to begin to yield at approximately 200 N given a yield

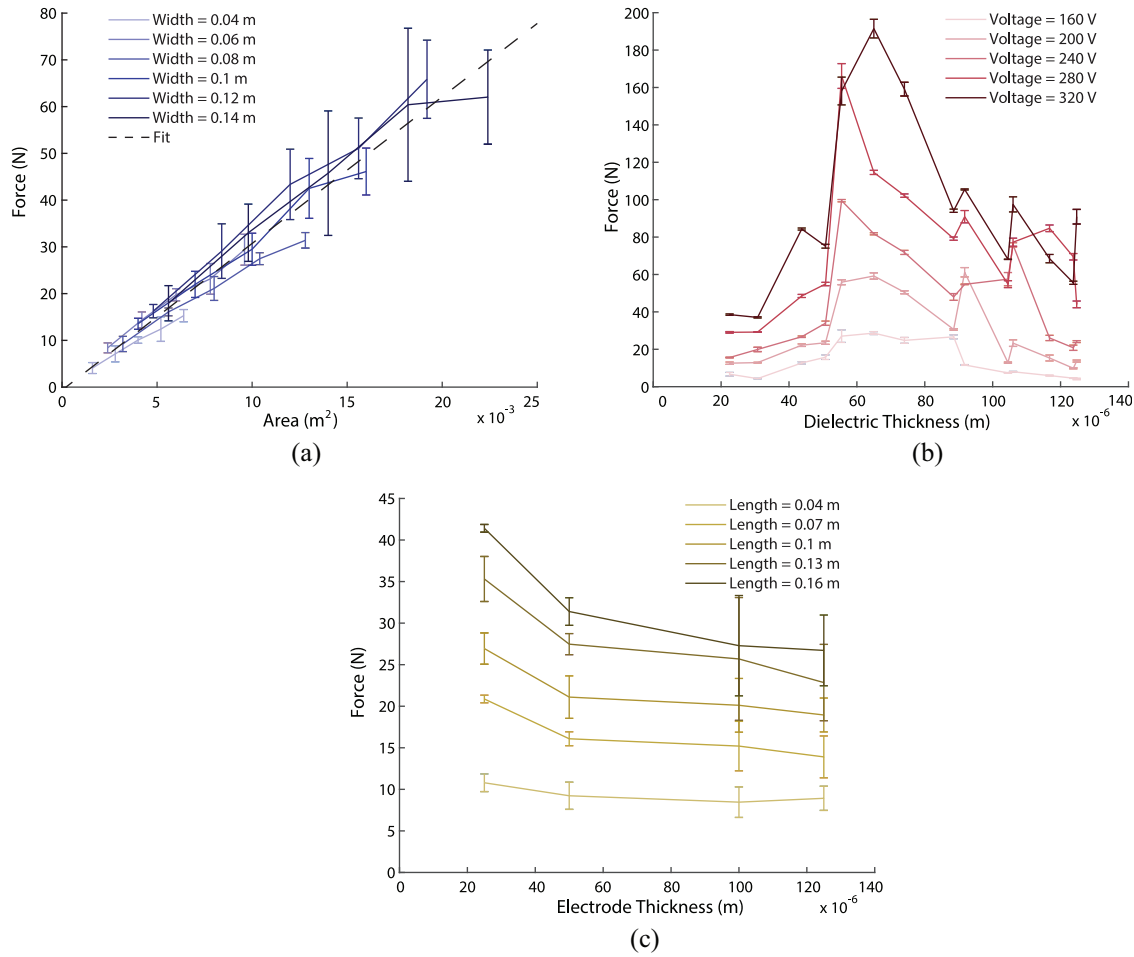


Figure 5. Maximum holding force results. (a) Maximum force as a function of area, with lines of constant width and applied voltage of 250 V. (b) Maximum force as a function of dielectric thickness, with lines of constant voltage and 50 μm electrode thickness. (c) Maximum force as a function of electrode thickness, with lines of constant length and applied voltage of 250 V.

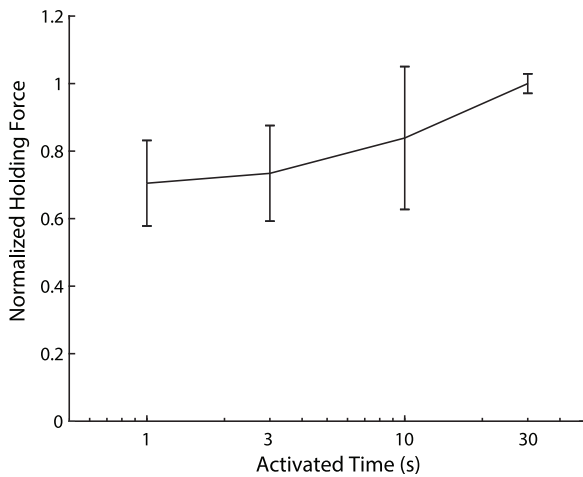


Figure 6. Normalized clutch holding force at 250 V as a function of the time between clutch activation and loading the clutch to slip. The clutch force is normalized to the slip force at the 30-s condition.

strength of 100 MPa (Dupont, 2017) at room temperature, which is only slightly larger than the measured slipping force of some clutches with 10 cm overlap length. Force can be expected to scale up or down linearly with the clutch overlap area, although clutch area has a strong effect on other performance outcomes, as is discussed in the “Release time” section. For all of the clutch designs tested in this article, the clutch slipped at the electroadhesive interface rather than experiencing a yielding failure in the materials or structure. Because the stress in the BOPET film and at the VHB interface scales inversely with clutch width for a given film thickness and overlap area, the clutch aspect ratio should be controlled during the design process by increasing width and decreasing length until the expected stress in the BOPET film is below the yield stress. Increasing voltage also increases clutch force, but has a strong effect on force hysteresis and power consumption, as discussed in sections “Space Charge” and “Power consumption.”

The holding force of clutches activated for 1 s is approximately 70% of the holding force after being activated for 30 s. The holding force does not appear to plateau after 30 s of activation time, implying that even higher forces may be reached with longer activation time. This result also shows that the electroadhesive clutch is capable of transmitting large holding forces within 1 s of activation. This time-dependent effect likely added some bias into the greater holding force parameter sweep experiment. Because the tests in the main holding force study were meant to be quasi-static, we tested at a low displacement rate. This meant that tests of parameter values that held large forces took up to 15 s longer than parameter values with low force capability, potentially causing a further relative difference in force transmitting capability. Additional tests of the interaction of displacement rate, activated time, and other clutch parameters such as voltage could give additional insight on the fundamental mechanisms underlying this effect.

Space charge. We also note several factors that affect performance but that we have not systematically investigated in this work. One such factor is that increasing voltage to 320 V and beyond begins to have detrimental effects on clutch performance. Specifically, we observe unwanted adhesion due to space charge, or electric charge that is forced into the insulating layer and remains even after the voltage is removed (Pourrahimi et al., 2018; Tian et al., 2011). Unwanted adhesion can be problematic when the clutch is in the off state, because the clutch plates buckle under very small compressive loads and consequently do not slide relative to one another. Quantifying the presence of space charge has proven to be a challenge. A remaining voltage is only observable with a voltmeter when the electrodes are slid relative to one another, and the transient nature

and strong history dependence of space charge make it difficult to systematically investigate its interaction with our performance outcomes. We have seen cases where suspected space charge induced by large voltages seems to temporarily slow release time and decrease maximum holding force. Further investigation into techniques of measuring space charge in our system and counteracting its effects are warranted.

Materials. Our selection of materials is vital to achieving good performance. Using aluminum-sputtered polymer film as the electrode provides the right combination of out-of-plane flexibility and high in-plane stiffness. The dielectric material choice is critical, and we use Luxprint, which is a fluoropolymer embedded with barium titanate and titanium dioxide, because it displays high breakdown strength and a high dielectric constant of approximately 20–30. In addition, this dielectric is not tacky and does not have inherent adhesion, meaning that the clutch can automatically release and reliably slide in the off state. The diameter of the ceramic particles is reported by the supplier to be less than 5 μm , but we believe the drop-off in performance at thicknesses less than 50 μm may be due to agglomerations of the particles on the order of ~ 10 μm (Figure 7). The presence of these agglomerations would lead to localized electric charge accumulation that could cause shorting and a lower bulk dielectric constant. Using a composite with smaller particles or chemical modification to prevent agglomeration could dramatically improve the performance of thinner layers and allow much lower applied voltage and higher force transmission.

Release time

Release time methods. The release time testing was also conducted using the Instron materials tester, but the

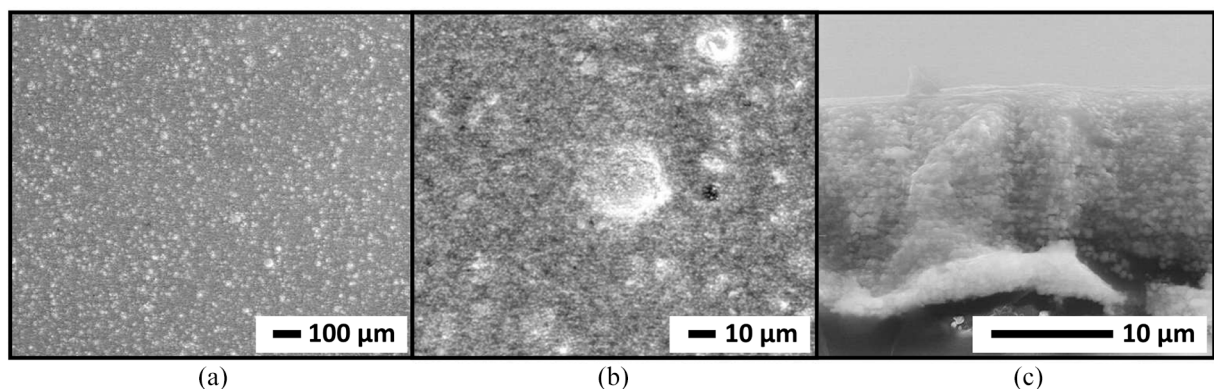


Figure 7. Environmental scanning electron microscope images. (a, b) Agglomerations of ceramic particles on the order of 10 μm are visible on the dielectric surface. Energy-dispersive spectroscopy analysis confirmed that the agglomerations are made up of barium titanate and titanium dioxide. (c) Cross-section of the dielectric layer. The individual ceramic particles are visible in the polymer matrix. All images were taken at 25 kV using a Quanta 200 (Thermo Fisher Scientific, Hillsboro, Oregon, USA).

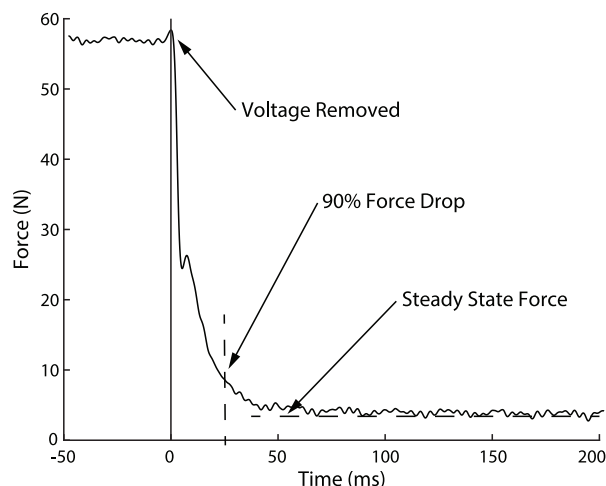


Figure 8. A representative force profile during release. After the voltage is removed from a clutch under load, the force rapidly drops to a steady-state value dependent on the force in the tensioning springs. We define the release time as the time required to drop to within 10% of the steady-state value. About halfway through the release, an inflection in the force profile occurs. This occurs in most releases and can vary significantly in its magnitude of force.

force was measured using a load cell (LC201-100; Omega, Norwalk, CT) placed in series with the clutch and recorded at 5000 Hz by a separate control hardware system (DS1103; dSPACE, Wixom, MI). A microcontroller (Arduino Uno, Somerville, MA) was used to control the clutch state and simultaneously send control state signals to the control hardware system. We chose not to use the Instron measurements because of embedded filtering, which prevents measurements on the millisecond scale, and because of software delays on the order of 10 ms. During each test, the clutch was activated, loaded to 80% of the measured or estimated maximum force, and released (Figure 8). At each condition, clutches were tested six times, with about 10 s between tests. Pilot testing did not show any change in performance over consecutive tests, so all six tests contributed to the dataset. The force signal was zero-phase 250 Hz low-pass filtered to eliminate background noise. We defined the release time as the time needed for the force to drop by 90% relative to the steady-state force after release. All clutches used in the force testing were also tested for release time under the same conditions, with the exception of the set of samples in which electrode thickness was varied. Rather than testing the interaction of electrode thickness and length as in the maximum holding force study, these samples were tested for the interaction of electrode thickness and voltage. The electrode thickness sweep samples were tested at an overlap length of 10 cm. Clutches were rested for at least 3 h between measurements. Real-time and high-speed video of release time testing can be viewed

in the “Electroadhesive Clutch Release and Engage Time Testing” video (Supplemental Material).

Release time results. Release time slows as area increases, and increasing clutch width increases the release time more sharply than increasing clutch length (Figure 9(a)). For dielectric thicknesses $\geq 80 \mu\text{m}$, release time becomes faster as dielectric thickness increases and applied voltage decreases (Figure 9(b)). The samples used in the sweep of electrode thickness have dielectric thickness of $36.6 \pm 3.9 \mu\text{m}$. With this in mind, considering Figure 9(b) and (c), the opposite trend appears to occur for thin samples with dielectric thickness $\leq 40 \mu\text{m}$. For this region, release time becomes faster as dielectric thickness decreases and applied voltage increases. For intermediate dielectric thicknesses, there is no clear relationship between release time and dielectric thickness or voltage. The outlying data in this region that shows very fast release time occur because of our definition of release time, and for practical purposes release at similar speeds to the other data at those dielectric thicknesses. The outliers occur because the small inflection at approximately 25 N in Figure 8 is much taller and actually dips below the 90% force drop value before rising and following the typical force profile. Future work is warranted to investigate the mechanics behind this feature of the force drop curve. Electrode thickness does not seem to have an effect on release time (Figure 9(c)), although the fastest release in this subset of clutches occurred for the 25- μm -thick electrode at 320 V.

Release time design insights. Based on the findings in Figure 9, the clutch area is the dominant design parameter in determining the release time. These findings imply that clutches with large continuous area or width cause slow release and should be avoided. This result leads us to consider other ways of scaling force while maintaining fast release time.

Increasing the continuous area of the clutch to increase force causes a corresponding increase in the time needed to release (Figure 10). The finding that width has a particularly strong effect on release time inspired an experiment in which we placed multiple clutches in parallel. When three clutches are loaded to 220 N and released, the release time is approximately the same as their individual release times when released at 70 N. This result implies that the continuous area of each clutch dominates release time, and additional clutch area and holding force can be added without penalty as long as it is not continuous area on a single clutch. To further explore this strategy, we cut slits along the length of one of the two clutch plates to decrease the continuous width to 1.3 cm and find that this dramatically reduces the release time of individual clutches as well as multiple clutches in parallel. This

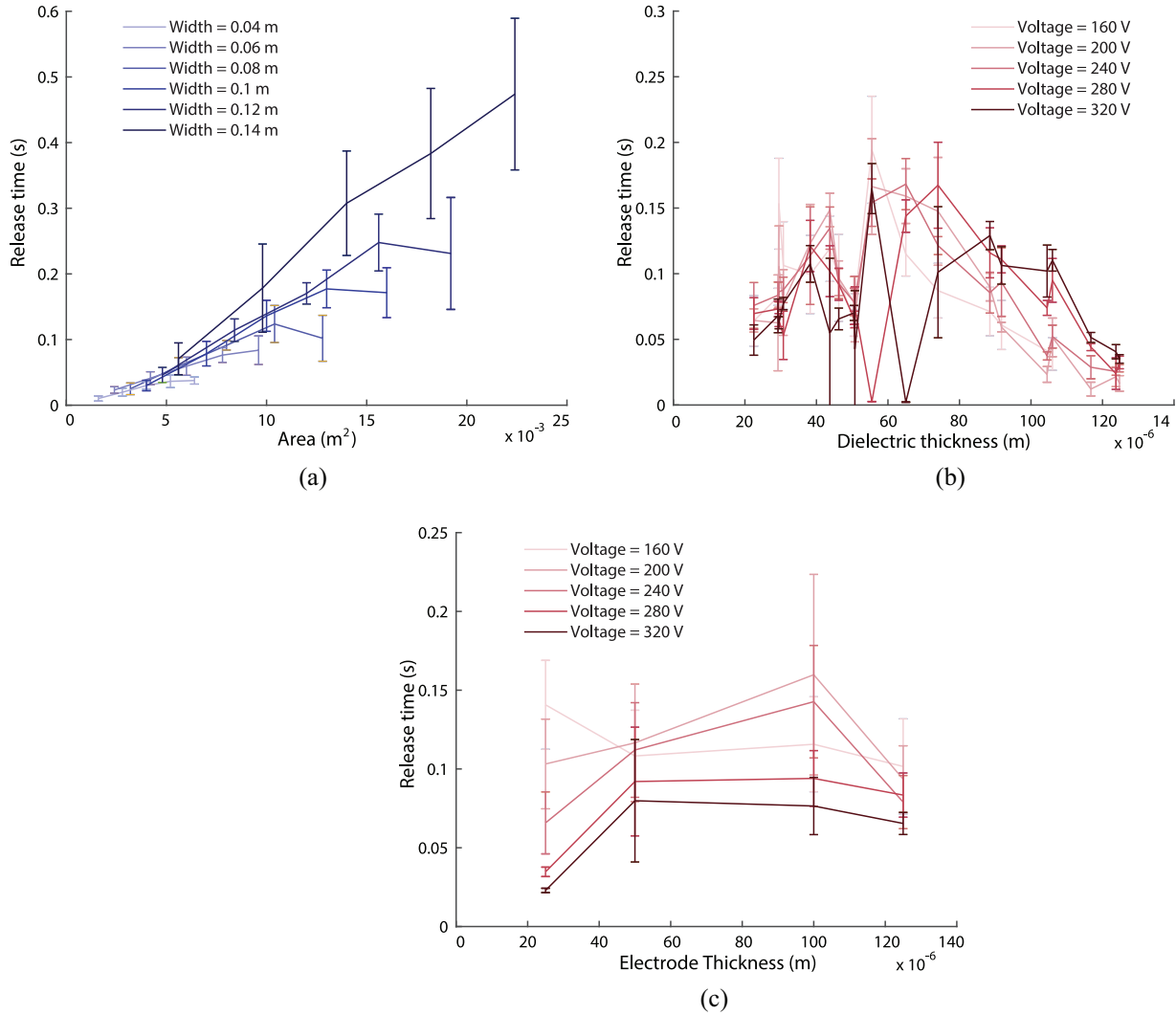


Figure 9. Release time results. (a) Release time as a function of area, with lines of constant width. (b) Release time as a function of dielectric thickness with lines of constant voltage. (c) Release time as a function of electrode thickness, with lines of constant voltage.

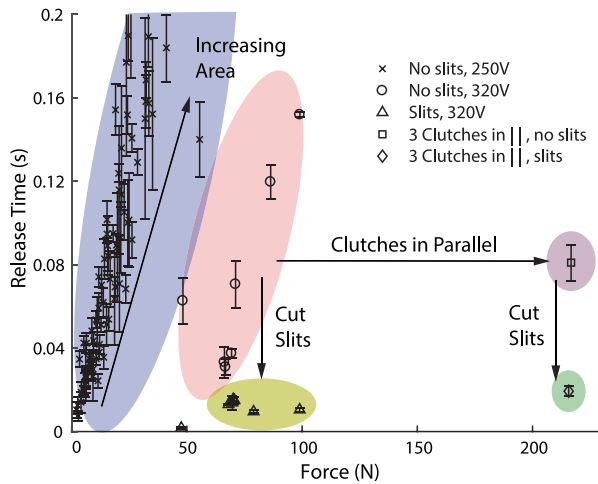


Figure 10. Release time and holding force. Scaling force by increasing area dramatically slows release time. Increasing voltage and using multiple smaller clutches in parallel scales force without sacrificing responsiveness, and cutting parallel slits in the clutches dramatically decreases release time.

result leads to the important design insight that continuous area in the clutch plates should be minimized in order to achieve fast release in clutches that can hold large forces.

Engage time

Engage time methods. The engage time was calculated by comparing a linearized baseline force–displacement curve to “dynamic engage” tests. During the dynamic engage test, the clutch was activated while being displaced at a constant rate (Figure 11). The amount of extension after the voltage was applied and before the clutch was fully engaged was determined by shifting the reference force–displacement curve until the force profile coincided with the dynamic engage curve. This extension shift correlated to a time value, because the dynamic test was conducted at a constant velocity. This time, which we called the engage time, is essentially the

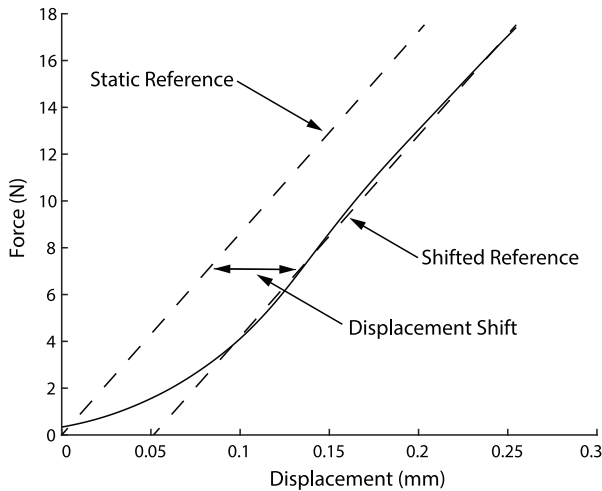


Figure 11. A representative force profile during engage. The voltage is applied at time zero, and the static reference line shows the expected force–displacement profile of a fully engaged clutch. By shifting the reference curve to the right until the curve coincides with the dynamic test, we determine the amount of displacement lost before the clutch is engaged. Because the velocity is constant, this displacement corresponds to a time value, which we call the “engage time.”

time needed for the stiffness of the engaging clutch to match its baseline stiffness.

Engage time measurements were also made with the Omega load cell and dSPACE system. In addition, the displacement was measured by dSPACE using the analog output of the Instron, which we separately verified did not have filtering or software delays. To determine the baseline force–displacement curve, the clutch was activated and loaded to 20 N at a rate of 100 mm/min. This test was repeated three times for each condition, and the final two tests were fit with a linear curve. The dynamic engage tests were performed by initiating an extension velocity of 100 mm/min, while the clutch was deactivated. Once constant velocity was reached, the microcontroller simultaneously engaged the clutch and signaled the measurement system, indicating the time and displacement at clutch activation. Voltage was provided by the high voltage power supply, and a 4.7- μ F capacitor was placed in parallel with the power supply to provide a responsive current source. The force and extension signals were both zero-phase low-pass filtered at 20 Hz. This filtering did not adversely affect our ability to measure fast engage times because we were not measuring an impulse-like behavior that would be masked by a low-pass filter. Instead, we measured the stiffness at a time well past the initial engage, and this part of the curve is very smooth. In addition, because we used a two-way filter, the curve was not delayed relative to the activation time. The dynamic engage test was performed four times per clutch at each condition, and all four tests contributed to the dataset. Parameter

sweeps of length, width, electrode thickness, and voltage were conducted for engage time, with three clutches tested at each condition. The clutches in the sweep of width had a mean dielectric thickness of $36 \pm 2.7 \mu\text{m}$, length of 13 cm, electrode thickness of 50 μm , and applied voltage of 280 V. The clutches in the sweep of length had a mean dielectric thickness of $37 \pm 2.6 \mu\text{m}$, width of 8 cm, electrode thickness of 50 μm , and applied voltage of 280 V. The clutches in the voltage sweep had a mean dielectric thickness of $31 \pm 0.9 \mu\text{m}$, overlap length of 13 cm, width of 8 cm, and electrode thickness of 50 μm . The clutches in the electrode thickness sweep had a mean dielectric thickness of $36 \pm 3.9 \mu\text{m}$, overlap length of 13 cm, width of 8 cm, and applied voltage of 280 V. The order of conditions was randomized for each clutch. Real-time and high-speed video of engage time testing can be viewed in the “Electroadhesive Clutch Release and Engage Time Testing” video (Supplemental Material).

Engage time results. Engage time decreases moderately as clutch width increases (Figure 12(a)). We believe that clutches with more area engage faster because there is a higher likelihood that some portion of the clutch plates will be in contact before activation to serve as an initiation point for zipping on. The engage time is quite dependent on the overlap length (Figure 12(a)), with the 10- and 16-cm conditions engaging most quickly. We believe this effect is due more to the clutch configuration and tensioners than to the absolute overlap length. The clutches used to test various lengths were created in two sizes, with maximum designed overlap lengths of 10- and 16-cm, and these clutches were activated in lengthened configurations to produce the 4-, 7-, and 13-cm conditions. However, these configurations have higher tensioner force than the 10- and 16-cm conditions, which we believe decreases the likelihood of initial contact and hinders the zipping on effect, leading to slower engage times. Clutches engage much faster as the applied voltage increases (Figure 12(b)), which is likely due to higher zipping forces at higher electric field strengths. Engage time occurs faster as the electrode thickness decreases, with the exception of the 100- μm clutches (Figure 12(c)). This outlier is most likely due to noticeable curvature in these samples resulting from residual stresses in the electrodes.

Engage time design insights. Clutch engage occurs faster for clutches with more area, potentially placing this performance measure at odds with the release time, which becomes slower as continuous area increases. However, engage time tests of clutches with slits show that they can engage within 30 ms, meaning that both fast engage and release can be achieved by employing slits. Using higher voltage and thinner electrodes benefits engage

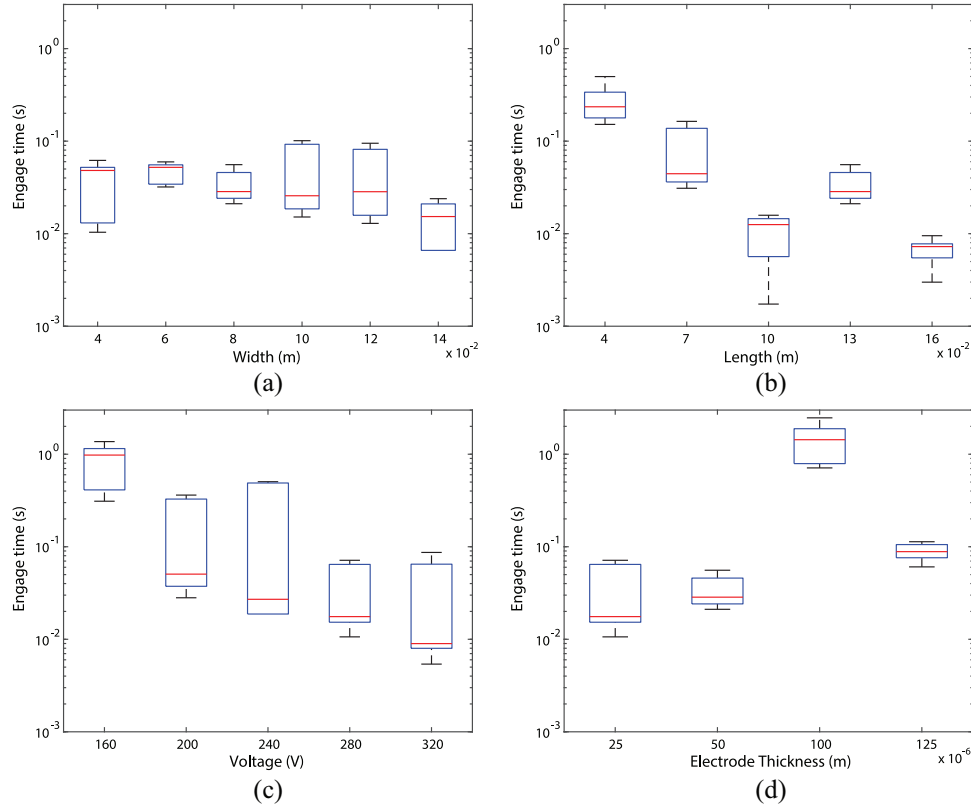


Figure 12. Engagement time results. These box-and-whisker plots show the median in red, the 25th and 75th percentiles with the blue box, and the most extreme data points with the whiskers. (a) Engagement time as a function of width. (b) Engagement time as a function of length. (c) Engagement time as a function of voltage. (d) Engagement time as a function of electrode thickness.

time, a result that meshes well with the force and release time results for these parameters.

The electrode thickness and length outliers in our engagement time data illustrate the dependence of engagement time on the curvature of the electrodes and the force from the tensioning rubber bands. The residual curvature in the clutches develops during fabrication and results from the thermal mismatch between the electrodes and insulating material, as well as uneven cooling rates after baking. Residual curvature induces elastic restoring forces in the films that cause the centers of the electrodes to be pushed away from one another. This can prevent the clutch plates from having any initial contact area, which is necessary for the electrodes to initiate adhesion. These effects were particularly pronounced in the 100- μm electrodes, perhaps due to the methods and processing performed by the BOPET manufacturers. This negative effect is exacerbated when vertical slits are cut for all electrode thicknesses, because the length-to-width ratio of the continuous patches dramatically changes, and the carbon fiber backing cannot as effectively constrain the electrode to be flat. We find that sliding the electrodes over a sharp edge before attaching them to the carbon fiber backing is an effective method to remove curvature. In fact, using this method to bias the curvature to the other

direction is actually beneficial in guaranteeing some initial contact area for engagement, allowing the electrodes to quickly zip on and conform to one another.

The force in the alignment tensioners also plays a role in determining the initial contact area of the clutches. If the force is too low, the electrodes can go slack and buckle away from one another. Alternatively, if the force is too high, the electrodes can be too taut and not contact one another at all. One way to ensure relatively constant tensioner force over the whole operating range is to use springs with fairly low stiffness and a significant pretension. Both the curvature and tensioners should be carefully designed in each implementation of the clutch. Fast engagement time is also aided by supplying a good current source, which we achieve by placing a high-voltage capacitor into the circuit. The capacitor slowly charges from the low-power voltage transformer and is capable of providing very high instantaneous current to the clutch, allowing full charging in milliseconds. Because the capacitor has orders-of-magnitude higher capacitance than the clutch, the overall voltage decrease resulting from charging the clutch is very low. These tension, curvature, and charging effects all significantly influence the speed and reliability of clutch activation and need to be carefully considered in each implementation.

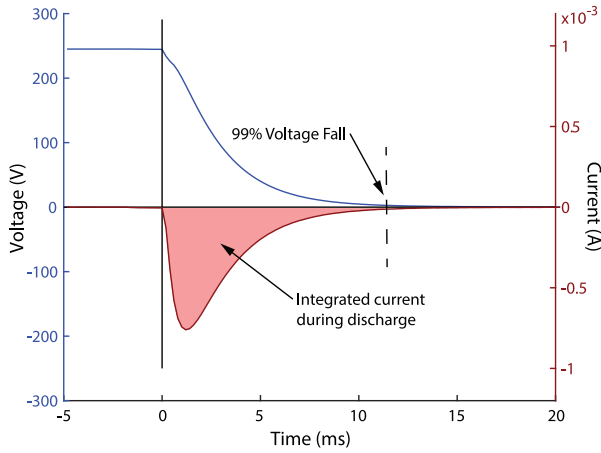


Figure 13. A representative clutch discharge curve. The voltage drops to 1% of its initial voltage within 12 ms. The current during discharge is integrated to determine the charge contained in the activated clutch.

Power consumption

Power consumption methods. We determined capacitance and power consumption of the clutches by charging and discharging clutches while measuring electrical current. Current was calculated by measuring the voltage drop across a 100-k Ω shunt resistor placed in series with the clutch, using two high voltage dividers (see the “Control circuits” section in Appendix 1). The electrical charge in the clutch was determined by numerically integrating the current during discharging (Figure 13). The clutch was considered to be discharging until the voltage across the capacitor had dropped by 99% of the applied voltage. The capacitance was then calculated as follows

$$C = \frac{Q}{V} \quad (2)$$

where Q is the total charge and V is the applied voltage. The leakage current during the charged state was also observed using this circuit. The power consumption was calculated using the measured capacitance and leakage current as

$$P = I_{\text{leak}} \cdot V \cdot D + \frac{1}{2} \cdot C \cdot V^2 \cdot f \quad (3)$$

where I_{leak} is the leakage current, D is the fraction of time the clutch is activated, C is the capacitance of the clutch, and f is the frequency of activation. For our calculations, we assumed an activation frequency of 1 Hz and an activation time fraction of 0.5.

Power consumption results. While varying clutch width, dielectric thickness, and electrode thickness, power consumption scales approximately linearly with maximum holding force (Figure 14(a)). This result makes intuitive

sense for varying width, as both force and capacitance scale linearly with clutch width. This is a surprising result, however, for varying dielectric thickness, as these results imply a linear relationship between capacitance and holding force that is not predicted by the friction-controlled electrostatic model, as described in the “Comparison of the empirical model to classic electrostatic theory” section. For these clutches, leakage current accounts for 22% of total power consumption on average, making it a relatively small cost compared to charging the clutches during activation.

The power consumption of a small subset of clutches was measured as a function of voltage (Figure 14(b)). Power consumption increases dramatically with increasing voltage, scaling as $V^{4.2}$, which is much higher than the prediction of V^2 from equation (3). This result can be explained by the dependence of clutch capacitance on clutch voltage (Figure 14(c)). Because the electrostatic pressure is higher at larger applied voltages, more of the air gap at the interface of the clutch plates is eliminated, effectively increasing the dielectric constant and decreasing the dielectric thickness. In addition, the high electric field strength may cause a nonlinear relationship between applied field and dielectric polarization that could contribute to this effect.

Power consumption design insights. Because of the relatively flat and linear data in Figure 14(a), power consumption does not require strong consideration when selecting the width, dielectric thickness, and electrode thickness of a design. Although using higher voltages quickly increases power consumption, the power consumption is not a hindrance to the implementation or practicality of the clutch. The estimated power consumption of the 65 μm clutch at 320 V is 3.2 mW, which is still very low compared to traditional clutches.

Fatigue life

Fatigue life methods. Fatigue tests were conducted by repeatedly loading and unloading the clutch. Each cycle was composed of a phase in which the clutch was activated, loaded, and then unloaded, followed by a “free-sliding” phase during which the clutch was displaced while the voltage was off, in order to ensure full disengagement of the clutch. The clutch was attached to a fixture with the Omega load cell in series, and a Kollmorgen (KM-180 E61960) servomotor displaced the free end. The dSPACE control system controlled the clutch activation circuit, and the high voltage power supply provided voltage, with a parallel capacitor acting as a current supply. The direction of applied voltage was alternated on each cycle. A controller was implemented to keep peak on-state force constant on each loading cycle (see the “Fatigue testing control” section in Appendix 1). The maximum force during the

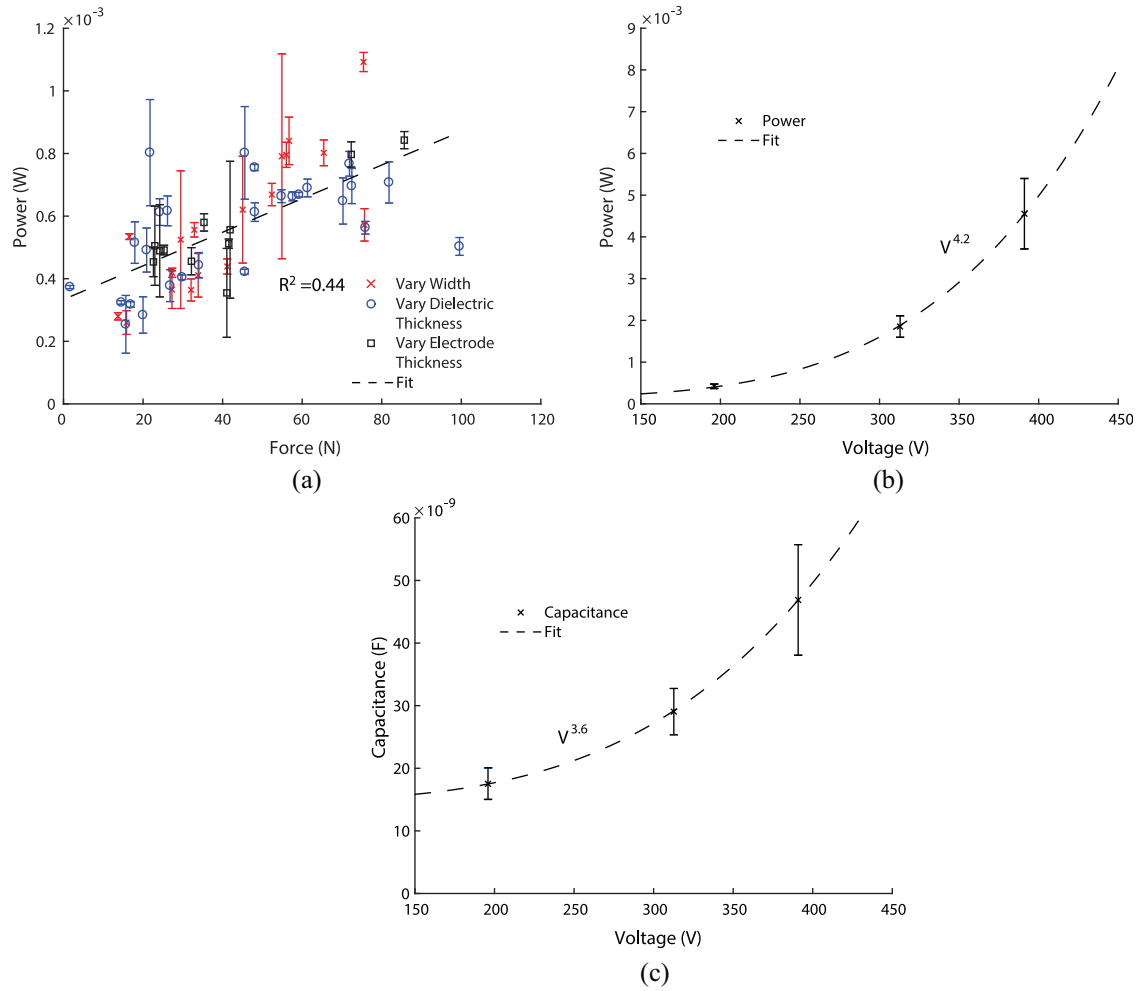


Figure 14. (a) Power consumption and maximum holding force. The “Vary Width” dataset includes clutches of various widths that have constant dielectric thickness and electrode thickness. The other two conditions follow the same pattern. (b) Power consumption as a function of applied voltage for three similar clutches. (c) Capacitance as a function of applied voltage for the same three clutches from (b).

off-state free-sliding cycle was also recorded, in order to investigate the unwanted residual adhesion as a function of cycle number. The off-state force was filtered to remove background noise, because a maximum value rather than an averaged value was recorded. Video of fatigue life testing can be viewed in the “Electroadhesive Clutch Fatigue Testing” video (Supplemental Material).

Fatigue life results. The fatigue testing results for one clutch are shown in Figure 15. The clutch performs more than 3.3 million loading cycles, with the clutch temporarily losing functionality 34 times, corresponding to approximately one loss in functionality per 100,000 cycles. The unwanted remaining adhesion of the clutch observed during the free-sliding phase starts at 0.5 N, but rises slowly during the course of the fatigue test, to a maximum value of 7 N. The clutch is able to restart within 5 s of a loss in functionality. Short

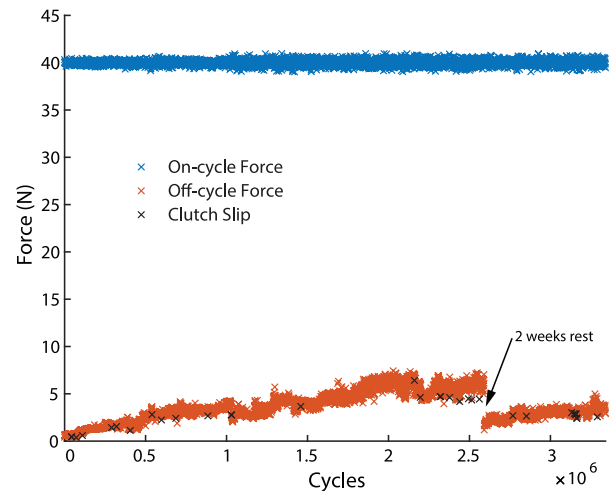


Figure 15. Fatigue testing. The maximum holding force and residual off-state force are plotted as a function of fatigue cycle number. The slip events are also indicated, overlaid on the off-cycle force of the cycle preceding the slip event. A 2-week break in testing is indicated with the arrow.

rests of less than 5 min do not seem to affect the unwanted off-state residual force upon restarting the test. However, a 2-week rest corresponded to a notable drop in residual adhesion of 4 N. The clutch shows very reliable operation for an extended usage time comparable to the requirements of many possible applications and demonstrates that there is no fundamental mechanism limiting the lifetime of electroadhesive clutches. However, further investigation is warranted to understand the failure mechanisms, the rise in residual adhesion, and how clutch life is related to fabrication methods. In addition, other performance outcomes including response time and power consumption should also be measured during fatigue testing.

Fatigue life design insights. To address residual adhesion in the off state for applications sensitive to this issue, the designer should consider replacing clutches after a few hundred thousand cycles, depending on their specific requirements. Further investigation could also inform techniques to delay or eliminate the rise in residual adhesion. Designers should include redundancy in the form of multiple parallel clutches to mitigate the loss in functionality when one clutch experiences a slipping failure. Including two clutches in parallel decreases the likelihood of a complete loss of force transmission to one in ten billion.

Data analysis

Analysis of variance and linear regression fitting

Model derivation methods. To extract key parameters and trends, we conduct an analysis of variance (ANOVA) analysis (Table 1). We find that clutch length, width, voltage, dielectric thickness, electrode thickness, and age have significant effects, while temperature, humidity, and test order do not. Clutch age is defined as the time between the last baking of the dielectric and the beginning of force testing. Temperature and humidity were not systematically varied during testing and typically stayed within 20°C–22°C and 20%–50% humidity. Test order was randomized. We used linear regression to determine exponent coefficients for a model including the statistically significant parameters described by the equation

$$F_x = \exp(c_1) \cdot l^{c_2} \cdot w^{c_3} \cdot t_d^{c_4} \cdot t_e^{c_5} \cdot V^{c_6} \cdot \text{age}^{c_7} \quad (4)$$

where l is the length of the clutch overlap area in meters, w is the width of the clutch overlap area in meters, t_d is the total dielectric thickness in meters, t_e is the thickness of each BOPET electrode in meters, V is the applied voltage in volts, and age is the clutch age in days (Table 2).

The coefficients were determined using a linear regression with $x = A^{-1}b$ where

Table 1. Recorded parameter statistical significance.

Parameter	p value
Length	4×10^{-8}
Width	2×10^{-4}
Dielectric thickness	3×10^{-11}
Electrode thickness	1×10^{-4}
Voltage	5×10^{-30}
Age	1×10^{-8}
Temperature	0.3
Humidity	0.4
Test order	0.7

Table 2. Fitted model coefficients for equation (8).

Coefficient	Thin subset	Full dataset	Thick subset
c'_1, c_1^*	−14.79		−23.18
c_2		0.9055	
c_3		1.103	
c'_4, c_4^*	−0.3829		−1.495
c_5		−0.3642	
c_6		2.612	
c_7		0.2901	

The center column gives coefficients derived from the full dataset. The thin and thick subset columns give coefficients derived from the respective subsets of data.

$$A = [1 \quad \ln(l) \quad \ln(w) \quad \ln(t_d) \quad \ln(t_e) \quad \ln(V) \quad \ln(\text{age})] \quad (5)$$

$$b = [\ln(F)] \quad (6)$$

$$x = [c_1 \quad c_2 \quad c_3 \quad c_4 \quad c_5 \quad c_6 \quad c_7]^T \quad (7)$$

From inspection, and consistent with findings from other electroadhesive force studies (Chen and Bergbreiter, 2017), we identify two regions of behavior in dielectric thickness (Figure 5(b)). We divide the data into thick dielectric and thin dielectric groups and alter equation (4) to include a distinct dielectric thickness term and constant multiplier for each group, where the cutoff thickness is selected to minimize the combined residual error of the model. The cutoff thickness is 53 μm . The new equation, which also includes distinct constant multipliers for the two groups of dielectric thickness, is as follows

$$F_x = \begin{cases} \exp(c'_1) \\ \exp(c_1^*) \end{cases} \cdot l^{c_2} \cdot w^{c_3} \cdot \begin{cases} (t'_d)^{c'_4} \\ (t_d^*)^{c_4^*} \end{cases} \cdot t_e^{c_5} \cdot V^{c_6} \cdot \text{age}^{c_7} \quad (8)$$

where c'_1 and c'_4 are the constant multiplier and dielectric thickness coefficient for the thin subset (t'_d), and c_1^* and c_4^* are the constant multiplier and dielectric thickness coefficient for the thick subset (t_d^*). The linear regression is performed in the same fashion as in equations

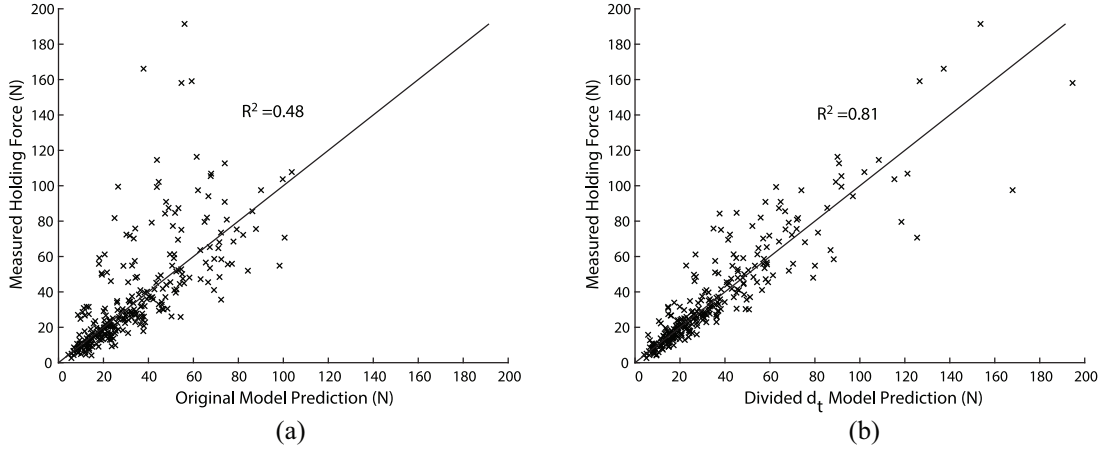


Figure 16. Maximum holding force model prediction vs measured data. (a) The model based on equation (4). (b) The model based on equation (8), with data divided by dielectric thickness. Partitioning dielectric thickness substantially improves the model prediction.

(5)–(7), with an additional two columns in the A matrix and two additional coefficients in the x matrix. In the new A matrix, the values in the columns corresponding to c'_1 and c'_4 are set to 0 for the thick subset data, and the values in the columns corresponding to c^*_1 and c^*_4 are set to zero for the thin subset data. This formulation separates the effects of dielectric thickness for the two groups and provides a necessary additional degree of freedom for each subset in the form of the constant multiplier while still considering the effects of all other parameters for both subsets as a single group. A prediction of holding force (in Newtons) for a particular set of design variables can be found by plugging the set of values into equation (8), ensuring that the units of l , w , t_d , and t_e are all meters, the unit of V is volts, the unit of age is days, and that the appropriate c_1 and c_4 are selected, given the selected dielectric thickness relative to the cutoff thickness of 53 μm .

Experimentally derived model of holding force. Providing the linear regression with additional degrees of freedom around dielectric thickness substantially improves the model prediction of holding force, increasing the R^2 from 0.48 to 0.81 (Figure 16). The original model underpredicts the highest measured force data (Figure 16(a)), an issue that is largely resolved in the modified model (Figure 16(b)).

By normalizing maximum holding force by the model prediction for all variables but one, we can visualize that variable's fit while accounting for all other effects (Figure 17). The model finds nearly linear increases in holding force as clutch length (Figure 17(a)) and width (Figure 17(b)) increase, with model coefficients of 0.91 and 1.1, respectively. Holding force scales as $(t_d^{-1.5})$ for the thick dielectric subset, while the thin dielectric subset is much flatter with respect to force, and is best fitted with $(t_d^{-0.38})$ (Figure 17(c)).

Increasing electrode thickness decreases force as $(t_e^{-0.36})$ (Figure 17(d)). Clutch voltage has the most dramatic effect on holding force, scaling force as $(V^{2.61})$ (Figure 17(e)). Finally, increasing clutch age causes a moderate increase in holding force, scaling as $(age^{0.29})$ (Figure 17(f)). While additional unknown effects likely contribute to the remaining error, this model does provide useful trends to inform design using the parameters investigated in this study.

Discussion

Optimal design values

Based on the results of the design study, we draw a few main design insights. Maximum holding force scales linearly with area, but increasing area, and width in particular, increases release time. Cutting slits to decrease continuous width greatly alleviates the release time penalty, and area can be increased without increasing release time by stacking smaller area clutches in parallel with one another. This is a critical design insight for applications requiring fast response, and we recommend keeping continuous area low by using slits and multiple clutches. Fast engage times are dependent on good alignment of the clutch plates, which is achieved by controlling clutch plate curvature during fabrication and selecting proper tensioners. Clutches perform best when the total dielectric thickness is between 50 and 80 μm . We recommend using the 25- μm electrode because it holds more force than the other thicknesses while having the lowest mass and volume. Finally, applying larger voltages greatly increases force, but dielectric breakdown and space charge impose practical limits on the voltage. Voltages near 300 V provide a good combination of high force, reliability, and responsiveness.

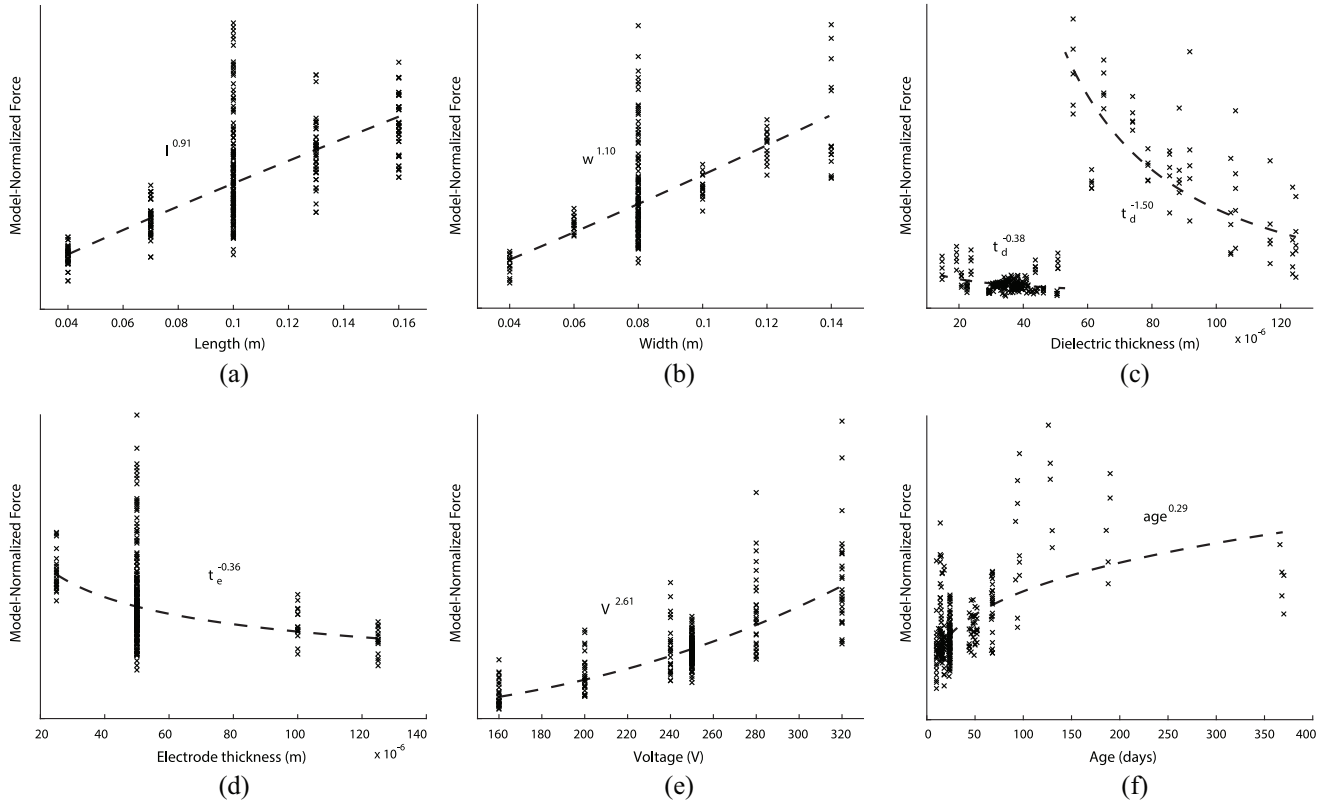


Figure 17. Maximum holding force normalized to each model parameter. In each plot, the y-axis value at the origin is zero. (a) Force normalized to length, (b) force normalized to width, (c) force normalized to dielectric thickness, (d) force normalized to electrode thickness, (e) force normalized to voltage, and (f) force normalized to age.

Comparison of the empirical model to classic electrostatic theory

One interesting comparison to our experimentally derived model is the electrostatic force theory for a parallel plate capacitor, given by equation (1). While this theory can describe some of the behavior we observed, it does not agree with many of our findings. The experimentally derived length and width scaling coefficients of 0.91 and 1.1 compare fairly well with the linear prediction of the electroadhesive clutch theory. A linear fit of the holding force versus clutch area in Figure 5(a) results in an R^2 value of 0.94. The slight deviation of these coefficients from a value of 1 may be due to geometric variations between clutches that become more detrimental as the clutch gets wider or longer, such as the position of attachment points. Such variations could impact load distribution, causing sub-optimal loading of regions near the edges of the clutch. The dielectric thickness coefficient of -0.38 for the thin subset deviates substantially from the theory prediction of -2 , indicating that the expected relationship between force and thickness is disrupted by other phenomena, such as breakdown, space charge, or non-uniformity on the micrometer scale. The scaling of dielectric thickness of -1.5 for the thick subset agrees better with theory, but is still lower than expected, potentially

due to some of the same phenomena. The model finds a coefficient of 2.6 for voltage, which is somewhat higher than the theory prediction of 2. This deviation is likely caused by improved adhesion and elimination of the air gap between the clutch plates at higher voltages, which would decrease the effective dielectric thickness and increase the charge in the electrodes. This larger value may also be due to the longer activated time of tests with large holding force, as discussed in the “Holding force design insights” section.

In a more pronounced disagreement with the model and data, the electrostatic theory underpredicts the overall magnitude of force produced in the clutch by a factor of 10. Fitting the thick dielectric data to electrostatic force theory with the coefficient ϵ as the free variable and our measured $\mu = 0.63$ (see the “Coefficient of friction testing” section in Appendix 1) produces an unrealistic dielectric constant of about 270, compared to our measured dielectric constant values of 15–20. In addition, the electrostatic force theory cannot account for the effects of electrode thickness and age. These disagreements between our experimental results and electrostatic force theory imply that this theory is not adequate for either qualitative or quantitative predictions of clutch performance, underscoring the importance of this and future experimental work.

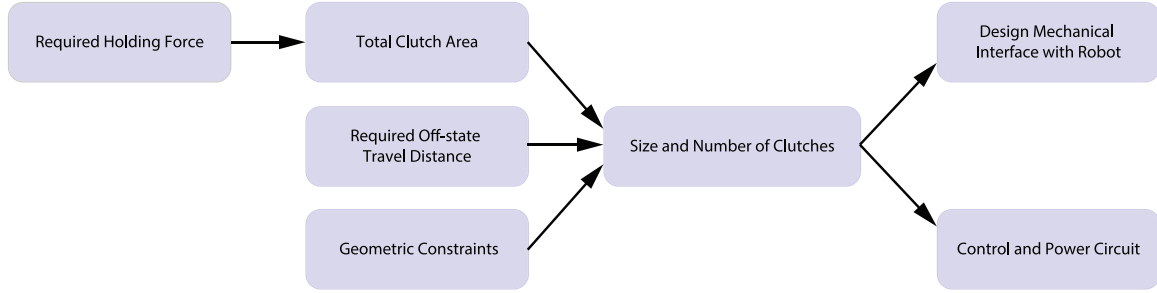


Figure 18. Design flowchart for electroadhesive clutch implementation.

The electrostatic force model relies on the assumption of dry Coulombic friction, which is inadequate for describing the adhesion interactions of thin polymer films. Other physical phenomena that may alter the critical shear force include van der Waals interactions, stiction effects, and geometric confinement (Bartlett and Crosby, 2013; Bartlett et al., 2012). The impact of these other effects has been shown in previous work, including for electrostatic adhesion. Chen and Bergbreiter (2017) observe increasing critical shear force in their soft electroadhesives as the ratio of width to thickness increases, which agrees with our finding that force increases as electrode thickness decreases for a constant width. Chen and Bergbreiter (2017) also measure critical shear forces up to three times higher than predicted by electrostatic force theory for the thinnest geometries. The authors do find that for certain width-to-thickness ratios, the measurements agree with electrostatic force theory. However, these correspond to aspect ratios that are 100–1000 times smaller than the range tested in this article. We are not able to make quantitative comparisons to this work because of differences in the materials, geometry, and methods, but this previous work finds similar trends to our findings. Given this set of previous work, it is not unreasonable and perhaps not even surprising that our clutch outperformed the electrostatic force theory.

Clutch age. The maximum holding force of the clutches increases as the clutches age. This may have to do with changes in the dielectric layer over time. One contributor may be continual evaporation of solvent that was not fully baked out of the dielectric during fabrication. It is possible the solvent decreases the overall dielectric constant of the insulating material and makes the clutch more susceptible to space charge, which we have observed can also decrease the maximum holding force. Further investigation of this phenomenon could inform changes to the fabrication process to compensate for this effect and achieve better performance of the clutches immediately after fabrication.

Design example

Appropriate clutch parameters can be selected based on the required holding force, total clutch travel, and the available space (Figure 18). First, the designers must determine the highest force that will be exerted by the clutch during operation. For example, in a lower-limb exoskeleton or legged robot application, the designers might place the clutch in series with a spring and stretch it to a maximum force of 1000 N. Using a factor of safety of 2, and our measured value of 23 kPa of shear pressure for a clutch with 65 μm dielectric thickness at 320 V, we calculate that 870 cm^2 of clutch area would be required. While this value may seem high, it can be accomplished in a compact device by stacking clutches in parallel with one another, as described later in this example. The next consideration is the required off-state travel distance of the clutch. In the hypothetical application, the designers might require 3 cm of travel in each direction from the neutral configuration during the off state. Next, geometric constraints must be taken into account. For the hypothetical device, the total length between the clutch attachments in the neutral configuration might be 14 cm. This would mean the clutch must shorten to a length of 11 cm and lengthen to a length of 17 cm. Factoring in 1 cm for the carbon fiber bars, this means the individual clutch plates could not be longer than 10 cm, or they would begin to buckle when the clutch is at its shortest length. Here, we define the clutch plate length as the distance from the attachment point to the edge of the clutch, as shown in Figure 19. In the hypothetical application, the designers may determine that they would typically want the spring to engage at a clutch length of 13 cm. The corresponding overlap length x can be determined using the equation

$$x = 2l_{cp} - L_t \quad (9)$$

where l_{cp} is the clutch plate length, and L_t is the total clutch length. Using clutch plates with individual lengths of 10 cm yields an overlap length of 7 cm. For the hypothetical application, the designers might assign

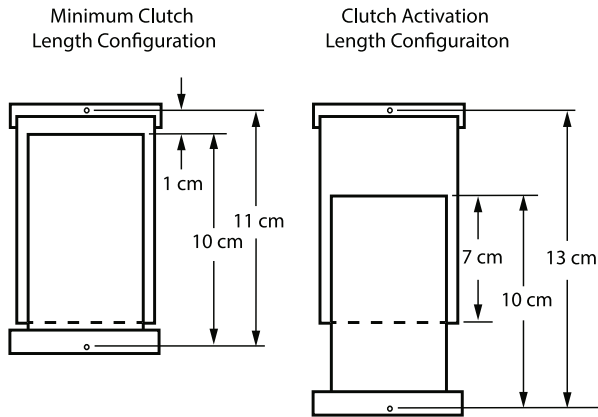


Figure 19. Clutch length diagram.

an 8-cm-wide space for the clutches. To allow space for tensioner spring attachments, the designers could then choose a clutch overlap width of 7 cm. This would correspond to an overlap area of 49 cm^2 per clutch, meaning that 18 clutches of this size would be necessary to transmit the required force.

To inform the sizing of electrical components, the designers could now estimate the steady-state power consumption of the clutches. If we assume the clutch is activated once per second with a duty factor of 50%, and the clutch has a dielectric thickness of $65 \text{ }\mu\text{m}$ and an applied voltage of 320 V, the power consumption is about $17 \text{ }\mu\text{W}$ per 1 N of force. Based on this scaling, the designers would estimate 34 mW of continuous power consumption. This means the designers would need to select a high-voltage transformer capable of outputting at least 34 mW continuously (e.g. the XPPower AG04N-5 DC-DC converter, which has a capacity of 1 W). In addition, the designers should place a capacitor in parallel with the transformer to reduce the peak current draw from the transformer and provide a good source for rapidly charging the clutches. The parallel capacitor should be relatively large compared to the total capacitance of the clutches (e.g. the Rubycon 400PX4.7MEFCTA8X11.5, which has a capacitance of $4.7 \text{ }\mu\text{F}$). All of the clutches could be controlled by a single control circuit requiring two high voltage relays (e.g. the Toshiba TLP222G-2, which can switch at up to 350 V). Together with low-voltage transistors, these electronic components would weigh less than 10 g and occupy less than 5 cm^3 .

Finally, the mechanical interface of the clutches with the robot structure would need to be considered. In our example, two clutch plates could be placed on each carbon fiber bar, for a total of nine bars per side. The bars could be 0.8-mm thick. Allowing for a 1-mm space between bars, the total thickness of the assembly would be 1.6 cm. It is important that the mounting allow for small rotations of the clutches during loading, as well as rotation about the mounting bolt to allow the clutches

to self-align into a state of pure tension. The carbon fiber bars should not be compressed together, and each bar should be able to move through a small range freely and independently.

The designers could approximate the expected mass of the clutches with the measured ratio for this dielectric thickness and voltage, which is 0.052 g per 1 N, resulting in an expected mass of 0.104 kg. The final assembly would have dimensions of $14 \text{ cm} \times 8 \text{ cm} \times 1.6 \text{ cm}$, corresponding to a volume of 179 cm^3 .

By comparison, a conventional clutch with comparable functionality for an exoskeleton or walking robot would have much higher weight and power consumption. An electromagnetic rotating tooth clutch capable of transmitting 108 N m would weigh about 1.5 kg, occupy a volume of 250 cm^3 , and consume 30 W of power when active (SEPAC, 2017). While the volume and responsiveness of this clutch would be comparable, it would weigh about 10 times more and consume about 500 times more energy than the electroadhesive clutch. Using a smaller clutch and a gearbox could also be problematic, because backdriving the gearbox would lead to undesirable torques due to the reflected inertia of the clutch and gearbox. For example, using a 100:1 gearbox would require the deactivated clutch to accelerate 100 times faster than the robot joint, leading to a reflected inertia of 10,000 times the original clutch inertia. In addition, any damping in the clutch during the off-state would be greatly magnified. Finally, planetary gearboxes capable of outputting 100 N m of torque commonly weigh on the order of 1 kg, and lighter alternatives such as lead screws are typically non-backdrivable. Achieving comparable functionality with a conventional electrically controllable clutch is simply not practical for most robotics applications, in terms of weight or energy consumption.

Applications

Electroadhesive clutches can provide many benefits while requiring only minimal added mass and power consumption. In their simplest implementation, clutches can lock degrees of freedom to reduce energy cost, enhance safety, or adjust passive dynamics. Many additional functionalities can be achieved by employing multiple clutches in various configurations (Van Ham et al., 2009). By placing a clutch in series with a spring, we can engage a passive force element when desired, with a controllable set point (Plooi et al., 2015). Adding more clutched springs in parallel provides adjustable stiffness (Diller et al., 2016). An actuator can operate with adjustable gear ratios or series stiffness when placed in series with clutched gearboxes and springs (Vanderborght et al., 2013). Attaching multiple clutches to a single spring can enable strain energy storage or provide a means to route energy between multiple degrees of freedom (Geeroms et al., 2013). Even

more complex systems of clutches, springs, and motors can provide many operation modes and functionalities (Leach et al., 2014; Plooij et al., 2017; Van Ham et al., 2009). These and other creative implementations could be applied to a broad range of applications, some examples of which we describe below.

Lightweight mobile robots. A particularly advantageous use case for electroadhesive clutches is the actuation of bipedal walking and running robots. Many of these robots seek to achieve spring-like leg behavior, with small amounts of energy injection or minor force profile variations for controlling balance (Hubicki et al., 2016; Ramezani et al., 2014). Because leg forces are high during stance, large motors or hydraulic pistons are commonly used (Johnson et al., 2015), even though the energy requirements for steady walking on level ground can be quite low (Collins et al., 2005; McGeer, 1990). In addition, fast low-force movement during the swing phase is desirable, leading to low gear ratios and larger actuators (Seok et al., 2012) or reductions in peak speed when actuator limits are encountered (Koolen et al., 2016). One solution is to place a spring in parallel with the actuator (Mazumdar et al., 2017), but this limits versatility and increases the difficulty of some movements (van Dijk and Van der Kooij, 2014). Using clutches to engage parallel springs only during desired periods, such as the stance phase of walking or running, would offload active elements, reducing their size or improving overall performance. Traditional clutches are too heavy and power-hungry to be practical for this purpose. By contrast, electroadhesive clutches and springs weighing just hundreds of grams and consuming less than 1 W of electricity can produce thousands of Newtons force while storing and returning hundreds of Joules of mechanical work (extrapolating from Diller et al., 2016). In addition, many robots could potentially incorporate clutches with relatively modest design changes. This actuation strategy could dramatically reduce the power consumption of existing robots and minimize the size and weight of actuators in future designs.

Implementing effective control strategies is a significant challenge for mobile robots, and limitations in possible actuator behavior contribute significantly to this problem (Cestari et al., 2014). Actuators with stiff transmissions can achieve high precision movement, but are typically non-backdrivable and can be dangerous to humans (Albu-Schaffer et al., 2007). Series elastic actuators, on the contrary, can execute torque control and interact with humans more safely, but sacrifice precision (Pratt and Williamson, 1995). A variable stiffness transmission based on electroadhesive clutches could enable mode-switching between a stiff connection for precise position control and a selectable series elasticity for enhanced torque control (Tonietti

et al., 2005; Zhang and Collins, 2017). For example, a humanoid robot's arm could perform precision manufacturing tasks with high repeatability using a stiff connection and position control and change modes to perform tasks in conjunction with humans more safely and naturally under torque control. This transmission would be lightweight and could change modes under load or in any configuration. Using a variable gearbox based on electroadhesive clutches could further enhance capability by expanding the possible torque/speed regime of the actuator, which can improve performance (Girard and Asada, 2016). Lightweight and responsive clutch-based transmissions could thereby improve the efficiency and capabilities of many mobile robots.

Exoskeletons, prostheses, and wearable devices. For exoskeletons and prostheses, low weight is a critical factor in achieving good performance. Adding mass to distal locations on the body causes a substantial increase in metabolic energy cost (Browning et al., 2007). Many existing devices have incorporated clutches or similar mechanisms in an attempt to reduce motor and battery size. For example, passive exoskeletons employing clutches and springs have assisted humans with walking (Collins et al., 2015; Walsh et al., 2007) and weight-lifting tasks (Yakimovich et al., 2009). Active exoskeletons and prosthetic limbs have incorporated variable stiffness joints and variable transmission ratios to adapt to user behavior (Blaya and Herr, 2004; Lenzi et al., 2017; Shepherd and Rouse, 2017). Clutch-like adjustments in prosthetic foot stiffness have been used to make step-by-step adjustments in ankle torque to enhance balance (Kim and Collins, 2017), and in exoskeleton damping to aid rehabilitation (Stegall et al., 2017). Assistive devices have used springs and multiple clutches to harvest energy from one joint to return it later or transfer it to another joint (Cherelle et al., 2017; Geeroms et al., 2013; Segal et al., 2012; Unal et al., 2010).

Energy-harvesting knee exoskeletons have used clutches to avoid interference during non-harvesting movements (Donelan et al., 2008). Clutches have been used as mechanical fuses, slipping when forces exceed a predetermined value to prevent a device from injuring the user (Lauzier and Gosselin, 2011). In each case, electroadhesive clutches could help overcome limitations imposed by the mass and energy consumption of traditional clutches or the constraints on versatility and controllability of mechanism-based approaches.

As the field of robotics continues to expand into non-industrial settings, electroadhesive clutches could help shape the development of assistive robots worn by people. Devices using online optimization (Ding et al., 2018; Koller et al., 2016; Zhang et al., 2017) might particularly benefit from the versatility of smart transmissions and actuators enabled by electroadhesive clutches.

Industrial robotics. Robots in manufacturing or other factory settings could also benefit from lightweight, low-power electroadhesive clutches. Many industrial robot arms require large actuators and high energy expenditure, in part to support their own weight. Attaching electroadhesive clutches and springs to joints could reduce the loads on actuators by providing gravity cancellation (Ulrich and Kumar, 1991; Vermeulen and Wisse, 2010). More energy savings could be achieved by actively adjusting the gravity cancellation set point (Herder, 2001; Morita et al., 2003). Incorporating many clutched springs in parallel with another would provide adjustable stiffness, allowing the gravity cancellation to adapt to changing weight at the end effector as parts are picked up and placed. Offloading actuators in this way could significantly reduce energy consumption or motor size and cost (Endo et al., 2010). Clutched springs could also store and return strain energy to quickly accelerate or decelerate a robot arm without requiring active actuator work (Babitsky and Shipilov, 2012; Plooij et al., 2015). Electroadhesive clutches could be beneficial in gripping or manipulation tasks, where they would lock an end effector after grasping an object to hold it at very low energy cost (Aukes et al., 2014; Kang et al., 2012). Introducing lightweight, low-power clutches to industrial settings could enable energy and cost savings with relatively minimal changes in hardware and manufacturing methods.

Applications summary. Incorporating electroadhesive clutches into actuator schemes would improve actuator performance and versatility while decreasing weight and power requirements. Electroadhesive clutches and springs can perform the energy-neutral portion of an actuation task, support body weight, or efficiently route force and energy across many degrees of freedom. Electroadhesive clutches can also expand actuator functionality through variable stiffness or variable mechanical advantage transmissions. By providing high force transmission and responsiveness at a fraction of the weight and power requirements of traditional clutches, electroadhesive clutches dramatically expand the possibilities for implementing responsive and adaptive hardware in robotic actuators.

Limitations. Our electroadhesive clutch design does have some drawbacks. The travel distance is constrained by the overall length and overlap length of the clutches, as well as the force in the tensioners in different configurations. In addition, the clutch could short in wet environments, necessitating a water-resistant casing for some applications. The clutch also has a limited temperature range of operation determined by the materials and likely has performance dependent on temperature and humidity, although we did not investigate such a dependence in this study. While these factors hinder use in

some implementations, we expect electroadhesive clutches will be an excellent option for a wide range of robotic applications.

Future work

Future investigation of clutch performance should include different loading rates, such as impulse loading on one extreme and creep detection on the other. Surface characterization could contribute to understanding the friction characteristics and true surface contact area achieved. Additional experiments should be conducted to understand the different mechanisms of force development at the interface, for example, by systematically varying the surface roughness of the dielectric layers. Further performance improvements could also come from investigation of the mechanism behind the clutch width's effect on force and release time. Finally, more systematic investigation of the effect of tensioner force and clutch curvature on clutch holding force and engage time should be conducted to produce quantitative design guidelines.

Conclusion

Electroadhesive clutches achieve orders-of-magnitude improvements in mass and power consumption compared to traditional clutches. In this work, we report a systematic investigation of electroadhesive clutch performance. The results of our study inform the design of clutches for a wide variety of usage cases according to their force, responsiveness, and power consumption requirements. Electroadhesive clutches have the potential to make hybrid actuation and passive actuation more feasible for robots in terms of weight, power consumption, and bandwidth.

Acknowledgements

The authors wish to thank Dr Maarten P. de Boer for the use of a high-speed camera and Bugra Kadri Ozutemiz for assistance with taking ESEM images.


Declaration of conflicting interests

The author(s) declared no potential conflicts of interest with respect to the research, authorship, and/or publication of this article.

Funding

The author(s) disclosed receipt of the following financial support for the research, authorship, and/or publication of this article: This work was funded by the National Science Foundation under grant IIS-1355716 and by a grant from Nike, Inc.

ORCID iD

Stuart B Diller  <https://orcid.org/0000-0003-3891-7351>

Supplemental Material

Supplemental material for this article is available online.

References

- Albu-Schaffer A, Haddadin S, Ott C, et al. (2007) The DLR lightweight robot: design and control concepts for robots in human environments. *Industrial Robot: An International Journal* 34(5): 376–385.
- Alkan MS, Gurocak H and Gonenc B (2013) Linear magnetorheological brake with serpentine flux path as a high force and low off-state friction actuator for haptics. *Journal of Intelligent Material Systems and Structures* 24(14): 1699–1713.
- Aukes DM, Heyneman B, Ulmen J, et al. (2014) Design and testing of a selectively compliant underactuated hand. *International Journal of Robotics Research* 33(5): 721–735.
- Awad MI, Gan D, Thattamparambil J, et al. (2016) Novel passive discrete variable stiffness joint (pDVSJ): modeling, design, and characterization. In: *Proceedings of the IEEE international conference on robotics and biomimetics (ROBIO)*, Qingdao, China, 3–7 December, pp. 1808–1813. New York: IEEE.
- Babitsky VI and Shipilov A (2012) *Resonant Robotic Systems*. Berlin: Springer Science & Business Media.
- Bartlett MD and Crosby AJ (2013) Scaling normal adhesion force capacity with a generalized parameter. *Langmuir* 29(35): 11022–11027.
- Bartlett MD, Croll AB, King DR, et al. (2012) Looking beyond fibrillar features to scale gecko-like adhesion. *Advanced Materials* 24(8): 1078–1083.
- Baser O, Demiray MA, Bas A, et al. (2017) A linear magnetorheological brake with multipole outer coil structure for high on-state and low off-state force outputs. *Turkish Journal of Electrical Engineering and Computer Sciences* 25(5): 3501–3514.
- Blaya JA and Herr H (2004) Adaptive control of a variable-impedance ankle-foot orthosis to assist drop-foot gait. *IEEE Transactions on Neural Systems and Rehabilitation Engineering* 12(1): 24–31.
- Boku K and Nakamura T (2010) Development of 3-DOF soft manipulator with ER fluid clutches. *Journal of Intelligent Material Systems and Structures* 21(15): 1563–1567.
- Browning RC, Modica JR, Kram R, et al. (2007) The effects of adding mass to the legs on the energetics and biomechanics of walking. *Medicine & Science in Sports & Exercise* 39(3): 515–525.
- Cestari M, Sanz-Merodio D, Arevalo JC, et al. (2014) ARES, a variable stiffness actuator with embedded force sensor for the ATLAS exoskeleton. *Industrial Robot: An International Journal* 41(6): 518–526.
- Chen AS and Bergbreiter S (2017) A comparison of critical shear force in low-voltage, all-polymer electroadhesives to a basic friction model. *Smart Materials and Structures* 26(2): 025028.
- Cherelle P, Grosu V, Flynn L, et al. (2017) The Ankle Mimicking Prosthetic Foot 3 Locking mechanisms, actuator design, control and experiments with an amputee. *Robotics and Autonomous Systems* 91: 327–336.
- Choi I, Corson N, Peiros L, et al. (2018) A soft, controllable, high force density linear brake utilizing layer jamming. *IEEE Robotics and Automation Letters* 3(1): 450–457.
- Collins SH, Ruina A, Tedrake R, et al. (2005) Efficient bipedal robots based on passive-dynamic walkers. *Science* 307(5712): 1082–1085.
- Collins SH, Wiggan MB and Sawicki GS (2015) Reducing the energy cost of human walking using an unpowered exoskeleton. *Nature* 522: 212–215.
- Diller S, Majidi C and Collins S (2016) A lightweight, low-power electroadhesive clutch and spring for exoskeleton actuation. In: *Proceedings of the IEEE international conference on robotics and automation (ICRA)*, Stockholm, 16–21 May, pp. 682–689. New York: IEEE.
- Ding Y, Kim M, Kuindersma S, et al. (2018) Human-in-the-loop optimization of hip assistance with a soft exosuit during walking. *Science Robotics* 3(15): 101126.
- Donelan JM, Li Q, Naing V, et al. (2008) Biomechanical energy harvesting: generating electricity during walking with minimal user effort. *Science* 319(5864): 807–810.
- Dupont TF (2017) *Mylar Polyester Film: product information*. Available at: http://usa.dupontteijinfilms.com/wp-content/uploads/2017/01/Mylar_Physical_Properties.pdf
- Elliott G, Sawicki GS, Marecki A, et al. (2013) The biomechanics and energetics of human running using an elastic knee exoskeleton. In: *Proceedings of the IEEE international conference on rehabilitation robotics (ICORR)*, Seattle, WA, 24–26 June, pp. 1–6. New York: IEEE.
- Endo G, Yamada H, Yajima A, et al. (2010) A passive weight compensation mechanism with a non-circular pulley and a spring. In: *Proceedings of the IEEE international conference on robotics and automation (ICRA)*, Anchorage, AK, 3–7 May, pp. 3843–3848. New York: IEEE.
- Furusho J, Sakaguchi M, Takesue N, et al. (2002) Development of ER brake and its application to passive force display. In: Bossis G (ed.) *Proceedings of the International Conference on Electrorheological Fluids and Magnetorheological Suspensions*. Singapore: World Scientific Publishing, pp. 57–62.
- Geeroms J, Flynn L, Jimenez-Fabian R, et al. (2013) Ankle-knee prosthesis with powered ankle and energy transfer for CYBERLEGS alpha-prototype. In: *Proceedings of the IEEE international conference on rehabilitation robotics (ICORR)*, Seattle, WA, 24–26 June, pp. 1–6. New York: IEEE.
- Girard A and Asada HH (2016) A practical optimal control approach for two-speed actuators. In: *Proceedings of the IEEE international conference on robotics and automation (ICRA)*, Stockholm, 16–21 May, pp. 4572–4577. New York: IEEE.
- Guo J, Bamber T, Singh J, et al. (2017) Experimental study of a flexible and environmentally stable electroadhesive device. *Applied Physics Letters* 111(25): 251603.
- Guo J, Elgeneidy K, Xiang C, et al. (2018) Soft pneumatic grippers embedded with stretchable electroadhesion. *Smart Materials and Structures* 27(5): 055006.
- Hawkes EW, Christensen DL, Pope MT, et al. (2016) One motor, two degrees of freedom through dynamic response switching. *IEEE Robotics and Automation Letters* 1: 969–975.

- Herder JL (2001) *Energy-free systems: theory, conception and design of statically balanced spring mechanisms*. PhD Thesis, Delft University of Technology, Delft, The Netherlands.
- Hubicki C, Grimes J, Jones M, et al. (2016) ATRIAS: design and validation of a tether-free 3D-capable spring-mass bipedal robot. *International Journal of Robotics Research* 35(12): 1497–1521.
- Hunt TR, Berthelette CJ and Popovic MB (2013) Linear one-to-many (OTM) system. In: *Proceedings of the IEEE international conference on technologies for practical robot applications*, Woburn, MA, 22–23 April, pp. 1–6. New York: IEEE.
- Inertia-Dynamics (2017) Flange Mounted Brakes—Type FB. Available at: <http://www.idicb.com/products/electromagnetic-clutches-and-brakes/brakes/type-fb>
- Johnson M, Johnson M, Shrewsbury B, et al. (2015) Team IHMC's lessons learned from the DARPA Robotics Challenge trials. *Journal of Field Robotics* 32(2): 192–208.
- Kakinuma Y, Aoyama T and Anzai H (2010) Development of high-performance ERG based on the principle of electro-adhesive effect. *Journal of Intelligent Material Systems and Structures* 21(15): 1501–1508.
- Kang H, Shim H, Jun BH, et al. (2012) Development of leg with arm for the multi-legged seabed robot “CR200.” In: *2012 Oceans*, Hampton Roads, VA, 14–19 October, pp. 1–4. New York: IEEE.
- Karagozler ME, Campbell JD, Fedder GK, et al. (2007) Electrostatic latching for inter-module adhesion, power transfer, and communication in modular robots. In: *Proceedings of the IEEE/RSJ international conference on intelligent robots and systems (IROS)*, San Diego, CA, 29 October–2 November, pp. 2779–2786. New York: IEEE.
- Kikuchi T, Otsuki K, Furusho J, et al. (2010) Development of a compact magnetorheological fluid clutch for human-friendly actuator. *Advanced Robotics* 24(10): 1489–1502.
- Kim M and Collins SH (2017) Step-to-step ankle inversion/eversion torque modulation can reduce effort associated with balance. *Frontiers in Neurobotics* 11: 62.
- Koller JR, Gates DH, Ferris DP, et al. (2016) “Body-in-the-loop” optimization of assistive robotic devices: a validation study. In: *Proceedings of the robotics: science and systems conference*, Ann Arbor, MI, 18–22 June.
- Koolen T, Bertrand S, Thomas G, et al. (2016) Design of a momentum-based control framework and application to the humanoid robot Atlas. *International Journal of Humanoid Robotics* 13(1): 1650007.
- Lauzier N and Gosselin C (2011) Series clutch actuators for safe physical human-robot interaction. In: *Proceedings of the IEEE international conference on robotics and automation (ICRA)*, Shanghai, China, 9–13 May, pp. 5401–5406. New York: IEEE.
- Leach D, Gunther F, Maheshwari N, et al. (2014) Linear multimodal actuation through discrete coupling. *IEEE Transactions on Mechatronics* 19(3): 827–839.
- Lenzi T, Cempini M, Hargrove LJ, et al. (2017) Actively variable transmission for robotic knee prostheses. In: *Proceedings of the IEEE international conference on robotics and automation (ICRA)*, Singapore, 29 May–3 June, pp. 6665–6671. New York: IEEE.
- Lord (2017) Lord TFD steering units. https://www.lord.com/sites/default/files/PB8130_TFDBrochure_2015-10-R2.pdf
- McGeer T (1990) Passive dynamic walking. *International Journal of Robotics Research* 9(2): 62–82.
- Mathijssen G, Furnemont R, Verstraten T, et al. (2016) +SPEA introduction: drastic actuator energy requirement reduction by symbiosis of parallel motors, springs and locking mechanisms. In: *Proceedings of the IEEE international conference on robotics and automation (ICRA)*, Stockholm, 16–21 May, pp. 676–681. New York: IEEE.
- Mazumdar A, Spencer SJ, Hobart C, et al. (2017) Parallel elastic elements improve energy efficiency on the STEPPR bipedal walking robot. *IEEE Transactions on Mechatronics* 22(2): 898–908.
- Morita T, Kuribara F, Shiozawa Y, et al. (2003) A novel mechanism design for gravity compensation in three dimensional space. In: *Proceedings of the IEEE international conference on advanced intelligent mechatronics*, Kobe, Japan, 20–24 July, pp. 163–168. New York: IEEE.
- Ogura-Industrial-Corp (2017a) OPB-N Electromagnetic Magnetic Brake. Available at: <http://ogura-clutch.com/products.php?category=2&product=88>
- Ogura-Industrial-Corp (2017b) VBEH / VBSH EM Brake (high torque design). Available at: <http://ogura-clutch.com/download.php?item=77&type=1>
- Plooi M (2015) Lock your robot: a review of locking devices used in robotics. *IEEE Robotics & Automation Magazine* 22(1): 106–117.
- Plooi M, van Nunspeet M, Wisse M, et al. (2015) Design and evaluation of the bi-directional clutched parallel elastic actuator (BIC-PEA). In: *Proceedings of the IEEE international conference on robotics and automation (ICRA)*, Seattle, WA, 26–30 May, pp. 1002–1009. New York: IEEE.
- Plooi M, Wolfslag W and Wisse M (2017) Clutched elastic actuators. *IEEE Transactions on Mechatronics* 22(2): 739–750.
- Pourrahimi AM, Olsson RT and Hedenqvist MS (2018) The role of interfaces in polyethylene/metal-oxide nanocomposites for ultrahigh-voltage insulating materials. *Advanced Materials* 30(4): 1703624.
- Prahlad H, Pelrine R, Stanford S, et al. (2008) Electro-adhesive robotswall climbing robots enabled by a novel, robust, and electrically controllable adhesion technology. In: *Proceedings of the IEEE international conference on robotics and automation (ICRA)*, Pasadena, CA, 19–23 May, pp. 3028–3033. New York: IEEE.
- Pratt GA and Williamson MM (1995) Series elastic actuators. In: *Proceedings of the IEEE/RSJ international conference on intelligent robots and systems (IROS)*, Pittsburgh, PA, 5–9 August, pp. 399–406. New York: IEEE.
- Ramezani A, Hurst JW, Hamed KA, et al. (2014) Performance analysis and feedback control of ATRIAS, a three-dimensional bipedal robot. *Journal of Dynamic Systems, Measurement, and Control* 136(2): 021012.
- Rossa C, Lozada J and Micaelli A (2014) Design and control of a dual unidirectional brake hybrid actuation system for haptic devices. *IEEE Transactions on Haptics* 7(4): 442–453.
- Rouse E, Mooney L and Herr H (2014) Clutchable series-elastic actuator: implications for prosthetic knee design. *International Journal of Robotics Research* 33(13): 1611–1625.
- Ruffatto D III, Shah J and Spenko M (2014) Increasing the adhesion force of electrostatic adhesives using optimized

- electrode geometry and a novel manufacturing process. *Journal of Electrostatics* 72: 147–155.
- Sakaguchi M, Furusho J and Takesue N (2001) Passive force display using ER brakes and its control experiments. In: *Proceedings of the IEEE international conference on virtual reality*, Yokohama, Japan, 13–17 March, pp. 7–12. New York: IEEE.
- Segal AD, Zelik KE, Klute GK, et al. (2012) The effects of a controlled energy storage and return prototype prosthetic foot on transtibial amputee ambulation. *Human Movement Science* 31(4): 918–931.
- Seok S, Wang A, Otten D, et al. (2012) Actuator design for high force proprioceptive control in fast legged locomotion. In: *Proceedings of the IEEE/RSJ international conference on intelligent robots and systems (IROS)*, Vilamoura, 7–12 October, pp. 1970–1975. New York: IEEE.
- SEPAC (2017) *RFTC series rotating field tooth clutch*. Available at: <https://sepac.com/products/view/rotating-field-tooth-clutch/#>
- Shafer AS and Kermani MR (2011) Design and validation of a magneto-rheological clutch for practical control applications in human-friendly manipulation. In: *Proceedings of the IEEE international conference on robotics and automation (ICRA)*, Shanghai, China, 9–13 May, pp. 4266–4271. New York: IEEE.
- Shan Y, Philen M, Lotfi A, et al. (2009) Variable stiffness structures utilizing fluidic flexible matrix composites. *Journal of Intelligent Material Systems and Structures* 20(4): 443–456.
- Shepherd MK and Rouse EJ (2017) The VSPA foot: a quasi-passive ankle-foot prosthesis with continuously variable stiffness. *IEEE Transactions on Neural Systems and Rehabilitation Engineering* 25(12): 2375–2386.
- Stegall P, Zanutto D and Agrawal SK (2017) Variable damping force tunnel for gait training using ALEX III. *IEEE Robotics & Automation Magazine* 2(3): 1495–1501.
- Tian F, Lei Q, Wang X, et al. (2011) Effect of deep trapping states on space charge suppression in polyethylene/ZnO nanocomposite. *Applied Physics Letters* 99(14): 142903.
- Toniatti G, Schiavi R and Bicchi A (2005) Design and control of a variable stiffness actuator for safe and fast physical human/robot interaction. In: *Proceedings of the IEEE international conference on robotics and automation (ICRA)*, Barcelona, Spain, 18–22 April, pp. 526–531. New York: IEEE.
- Ulrich N and Kumar V (1991) Passive mechanical gravity compensation for robot manipulators. In: *Proceedings of the IEEE international conference on robotics and automation (ICRA)*, Sacramento, CA, 9–11 April, pp. 1536–1541. New York: IEEE.
- Unal R, Behrens SM, Carloni R, et al. (2010) Prototype design and realization of an innovative energy efficient transfemoral prosthesis. In: *Proceedings of the IEEE international conference on biomedical robotics and biomechanics (BioRob)*, Tokyo, Japan, 26–29 September, pp. 191–196. New York: IEEE.
- van Dijk W and Van der Kooij H (2014) XPED2: a passive exoskeleton with artificial tendons. *IEEE Robotics & Automation Magazine* 21(4): 56–61.
- Van Ham R, Sugar TG, Vanderborght B, et al. (2009) Compliant actuator designs. *IEEE Robotics & Automation Magazine* 16(3): 81–94.
- Vanderborght B, Albu-Schaffer A, Bicchi A, et al. (2013) Variable impedance actuators: a review. *Robotics and Autonomous Systems* 61(12): 1601–1614.
- Vermeulen M and Wisse M (2010) Intrinsically safe robot arm: adjustable static balancing and low power actuation. *International Journal of Social Robotics* 2(3): 275–288.
- Walsh CJ, Endo K and Herr H (2007) A quasi-passive leg exoskeleton for load-carrying augmentation. *International Journal of Humanoid Robotics* 4(3): 487–506.
- Wu WJ and Lin PC (2017) A switchable clutched parallel elasticity actuator. In: *Proceedings of the IEEE international conference on advanced intelligent mechatronics*, Munich, 3–7 July, pp. 1173–1178. New York: IEEE.
- Yakimovich T, Lemaire ED and Kofman J (2009) Engineering design review of stance-control knee-ankle-foot orthoses. *Journal of Rehabilitation Research and Development* 46(2): 257–267.
- Zhang J and Collins SH (2017) The passive series stiffness that optimizes torque tracking for a lower-limb exoskeleton in human walking. *Frontiers in Neurorobotics* 11: 68.
- Zhang J, Fiers P, Witte KA, et al. (2017) Human-in-the-loop optimization of exoskeleton assistance during walking. *Science* 356(6344): 1280–1284.

Appendix I

Control circuits

The control circuits used for experimental testing are shown in Figure 20. Both circuits include a 4.7- μF capacitor (400PX4.7MEFCTA8X11.5, Rubycon), which was slowly charged up using the high-voltage power supply (Model PS375; Stanford Research Systems) before testing began. This capacitor, which has approximately 100 times higher capacitance than the clutch, provided larger instantaneous currents during clutch activation than the power supply is capable of, and smoothed the current draw from the power supply. The maximum holding force, release, engage, and fatigue tests were conducted using the circuit in Figure 20(a). For the majority of the fatigue tests, the high voltage was provided by a DC high voltage transformer (AG-05 Proportional Converter, EMCO). In both circuits, the photocoupler relays (TLP222G-2, Toshiba) are individually activated to control the voltage applied to each clutch plate. Each pair of relays can be controlled to put the clutch plate at high voltage, ground, or floating states. When a clutch plate changes from high voltage to ground, or vice versa, a 1-ms delay is observed between deactivating one relay and activating the other, in order to prevent shorting, which would occur if the clutch plate was connected to both high voltage and ground simultaneously. The circuit in Figure 20(b) was used to measure clutch capacitance and power consumption. A 100-k Ω shunt resistor was placed in series with the clutch, and two high-impedance voltage dividers were placed on either side to measure the voltage drop. The voltage dividers stepped the voltage down by a factor of approximately

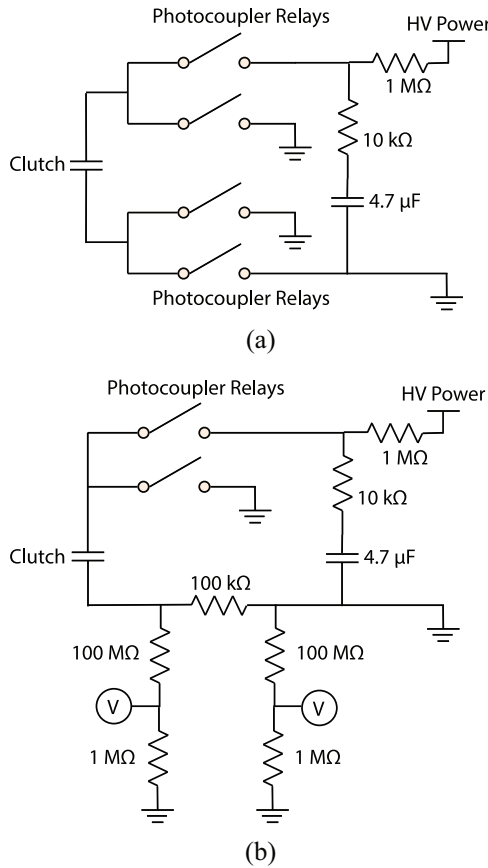


Figure 20. Circuit diagrams. (a) Control circuit for maximum holding force, release, engage, and fatigue tests. (b) Control circuit for capacitance and power consumption tests.

100, to allow voltage measurement using the dSPACE control system. The current loss through the voltage dividers was on the order of microamps and was compensated for in the current calculations.

Fatigue testing control

For control purposes, the control system measured motor position and clutch force at 1000 Hz and recorded the averaged force data at peak force for inclusion in the data recording, in order to reduce data file size. The control system also commanded motor velocity to the motor controller. An iterative learning control law was implemented to compensate for break-in and changing slack in the system and maintained a constant maximum clutch force from cycle to cycle. The commanded motor velocity V was a function of the average of the last five commanded velocities, a proportional error term, and a damping term, according to

$$V_n = \frac{\sum_{i=1}^5 V_{n-5n-1}}{5} + k_p * (F_{des} - F_{n-1}) + k_d * (V_{n-1} - V_{n-2}) \quad (10)$$

where F_{des} is the desired peak clutch force, k_p is the proportional gain, and k_d is the damping coefficient. In order to prevent position drift, a similar iterative learning controller was implemented to control the return stroke of the free-sliding phase, with a desired ending motor position of 0. On each cycle, the clutch was allowed 400 ms to engage before loading and 300 ms to disengage before the free-sliding phase. This resulted in a full cycle frequency of approximately 0.55 Hz. As a safety limit, the test stopped if the commanded motor velocity during the loading phase surpassed twice the nominal value, which only occurred in cases where the clutch repeatedly slipped and was unable to achieve the desired peak force on multiple consecutive cycles. The clutch was rested for various amounts of time after the test stop was triggered by multiple slips, in order to understand the effect of rest time on the ability to recover functionality. The minimum rest time was 5 s, and the clutch was always able to recover functionality after each rest. Cycles where the clutch maximum force was outside the range of 39–41 N were excluded, in order to prevent counting cycles during force ramp-up at the beginning of tests and after slip cycles. This strategy resulted in the exclusion of 0.1% of the total cycles.

Coefficient of friction testing

The coefficient of friction of the Luxprint-on-Luxprint interface was measured by stacking a known weight onto a pair of electrodes and slowly ramping lateral force by hand until a slip occurred. One electrode was held stationary on the table, and a load cell attached to the other electrode measured the force at slip. A thin sheet of rubber was placed between the stationary electrode and the table, and a separate sheet of rubber was placed between the other electrode and a flat metal

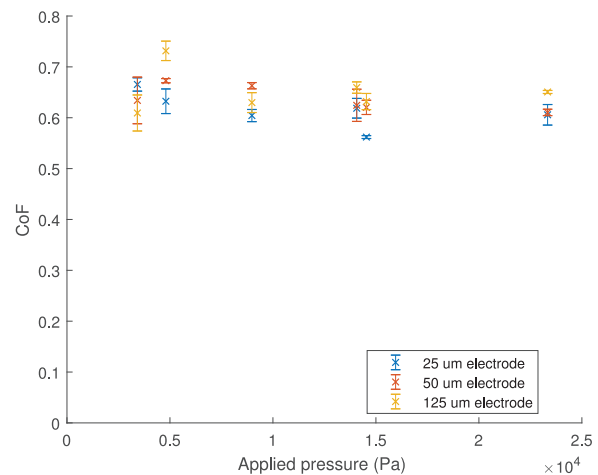


Figure 21. Coefficient of friction testing. The coefficient of friction is constant across a range of applied pressures and electrode thicknesses.

plate, in order to ensure uniform load distribution. Weights were then stacked onto the metal plate. The coefficient of friction was determined for each trial using the equation

$$\mu = \frac{F_{slip}}{F_{normal}} \quad (11)$$

where μ is the coefficient of friction, F_{slip} is the measured force at slip, and F_{normal} is the weight stacked onto the electrodes. Three pairs of electrodes, each with different electrode thicknesses, were tested at a range of pressures between 3 and 23 kPa. The coefficient of friction was 0.63 ± 0.04 and was constant across the whole range of applied pressures (Figure 21).